Sacks, I.S., Suyehiro, K., Acton, G.D., et al., 2000
Proceedings of the Ocean Drilling Program, Initial Reports Volume 186

1. Leg 186 Summary[1]

Shipboard Scientific Party[2]

ABSTRACT

Two borehole geophysical observatories were installed ~1100 meters below seafloor (mbsf) on the deep-sea terrace of the Japan Trench during Ocean Drilling Program (ODP) Leg 186. Site 1150 (39°11′N, 143°20′E) and Site 1151 (38°45′N, 143°20′E) are located in areas with contrasting seismic characteristics. The northern site is within a seismically active zone where microearthquakes are frequent and M7 earthquakes recur. The southern site is within an aseismic zone where no microearthquakes are observed. These features coexist within the seismogenic zone of the Japan Trench plate subduction zone, where the >100-Ma portion of the Pacific plate is subducting at a fast rate (~9 cm/yr) beneath northern Japan causing major earthquakes along the trench. Such a dynamic nature of the subduction seismogenic zone remains unexplained because no geodetic and few seismic stations exist on the seafloor that give us relevant observations in the vicinity of the fault (décollement) zone. Leg 186 is the first scientific venture to succeed in installing state-of-the-art strain, tilt, and seismic sensors for long-term operation in seafloor boreholes. The borehole instruments were installed only 10 km above the gently dipping (<5°) plate boundary. The systems will start collecting data in September 1999 and will be serviced by a remotely operated vehicle (ROV) at least once a year to recover continuous high sampling rate and wide dynamic range data. These stations will make invaluable additions to the existing geophysical network over the western Pacific. This type of multiple-sensor seismo-geodetic observatory can now be emplaced by the *JOIDES Resolution* at many other areas where active processes wait to be monitored.

Previous drilling in the area took place during Deep Sea Drilling Project (DSDP) Legs 56, 57, and 87, which transected the Japan Trench at ~39.8°N–40.7°N. These legs established the concept of tectonic erosion along a subduction zone. The Neogene subsidence history of the

[1]Examples of how to reference the whole or part of this volume.
[2]Shipboard Scientific Party addresses.

Ms 186IR-101

forearc was documented, and numerous ash records were obtained that span the past 9 m.y. The coring and logging data obtained from Sites 1150 (2681-m water depth) and 1151 (2182-m water depth) provide additional observations to further our understanding of the tectonics of this area with better recovery and higher resolution than was available from previous drilling along the Japan Trench. The ages of the recovered sediments are 10–0 Ma at Site 1150 and 16–0 Ma at Site 1151. The sedimentation rates between the two sites are broadly similar after 8 Ma and are consistent with those reported at DSDP Leg 57 Site 438 and Leg 87 Site 584 but differ before 8 Ma.

Estimations on the deformational history from observed microfractures and microfaults and logging data are consistent with a general east-west extensional stress field in which normal faulting dominates. It will be of great interest to compare these structural data and additional mechanical properties measurements to be made on whole-round core samples with data from the observatories, where the current tectonic stress field is actually east-west compressional across the Japan arc to the Sea of Japan.

Recovering detailed ash records was one of the highlighted drilling objectives. As with previous drilling results, a general increase from ~9 Ma and a peak in the past 0.5–4 m.y. are observed at the two sites. Postcruise studies will examine the details of the ash record, which was more completely recovered during Leg 186 than on previous cruises.

Inorganic geochemical analysis confirmed that a large decrease in chlorinity and salinity with depth exists in the Japan Trench region. This was first observed at DSDP Sites 438 and 439 but not at other sites of Legs 56 and 57. The character of the anomalies varies also between the two ODP Leg 186 sites. Overall, the magnitude of decrease seems much larger than other subduction environments such as at Nankai, Leg 131, or Barbados, Leg 171A.

To further our understanding of the plate subduction dynamics, near-site multiple disciplinary investigations are clearly needed. In particular, geological "hysteresis" concealed in present-day dynamics needs to be better understood to construct physical models by linking geological/geochemical and geophysical studies. Leg 186 is one such investigative attempt to link current and past dynamics by establishing borehole observatories and by obtaining core and logging data at the seismogenic zone of the Japan Trench.

INTRODUCTION

The scientific importance of establishing long-term geophysical stations in deep oceans has been acknowledged by earth sciences and ODP communities and is expressed in various articles (COSOD II, 1987; Purdy and Dziewonski, 1988; BOREHOLE, 1994; Montagner and Lancelot, 1995; Ocean Drilling Program, 1996). Indeed, more than a few important inferences on the dynamics of the Earth's deep interior have been inferred from seismic tomography images, such as the existence of super plumes, deep continental roots, stagnation of subducting plates within the mantle, and variations in the thickness of the thermal boundary layer at the base of the mantle (e.g., Fukao, 1992). Detailed examination of active processes at plate boundaries has also brought about significant inferences on magma reservoirs at oceanic ridges and on the décollement structure of subducting plates.

In essence, we wish to understand active processes driving Earth's dynamics from a global to a regional scale. A major step forward will almost certainly be made by installing permanent observatories in the oceans, which constitute 71% of Earth's surface. Obtaining observations from oceanic areas is significant not only for global coverage, but because most of the plate boundaries exist beneath the oceans, particularly those boundaries where oceanic lithosphere is presently being generated and recycled.

The western Pacific area is ideal for addressing problems related to plate subduction. In particular, the Japan Trench area is where much effort has been made for monitoring seismic and geodetic motions on land for many years. Together with marine geological and geophysical investigations on both sides of the Japan island arc, this area probably is the best studied subduction area. The area can be characterized as having a fast subduction rate and being a seismically active and well-coupled area. We also have knowledge of the sedimentary and tectonic environment from previous drilling, which found the forearc area to be subsiding as a result of tectonic erosion with little accretionary prism development.

To monitor strain and seismic activity continuously and ultimately to understand how plate motion is accommodated across a subduction zone, we have installed two geophysical observatories on the landward side of the Japan Trench (Fig. F1). Coring and logging data collected during the cruise are also expected to provide a tectonic history that can be linked to the present dynamics, which will be inferred from the observatories.

Although not always the case, normal coring objectives and observatory objectives often overlap and are interrelated as in this leg or recent Circulation Obviation Retrofit Kit legs. Once an observatory is established, ways and means to recover the data and to keep the station running become necessary. Such tasks are not easily undertaken even if a site only needs servicing once a year. A new fiber-optic cable owned by the University of Tokyo already exists and currently terminates near Site 1150. Once Site 1150 proves to be functioning, connections will be made to supply power, send commands, and retrieve data in real time on land. Furthermore, a 50-km cable extension is planned to connect Site 1151 as well. These stations will make invaluable additions to the existing geophysical network over the western Pacific. The data will eventually become accessible worldwide through the Internet.

F1. Location of Leg 186 sites, p. 19.

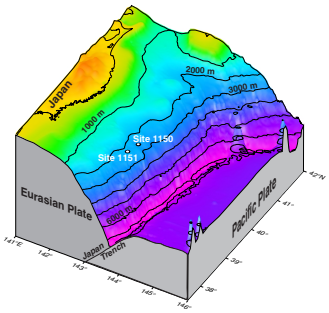

PREVIOUS DRILLING ALONG THE JAPAN TRENCH

Previous deep-sea drilling sites along the Japan Trench are shown in Figure F2. During DSDP Legs 56 and 57, Sites 436 (Leg 56), 434 (Leg 56), 441, 440, and 435 (Leg 56) were drilled along seismic Line JNOC-2 across the trench at 39°45'N. Sites 438 and 439 were drilled along seismic Line JNOC-1 across the trench at 40°40'N (Scientific Party, 1980). During DSDP Leg 87, Site 584 was also drilled in the area (Kagami, Karig, Coulbourn, et al., 1986). These legs were focused on the study of the mechanism and dynamics of plate convergence and their effects on sedimentation. It is presently widely accepted that little tectonic accretion is occurring. Instead, a massive subsidence has been taking place along the Japan Trench. This was a surprising finding substantiated by past drilling. Another surprise was the unexpected discovery of andesitic volcanic rocks from Site 439, 90 km from the trench axis, which in-

F2. Map of the Japan Trench area off northeast Japan, p. 20.

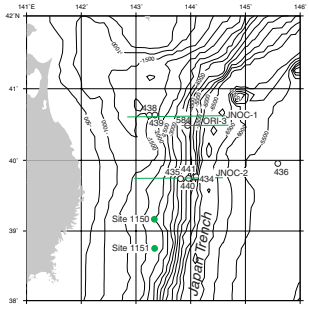

dicated that there is an offset of ~200 km between the present arc and where Oligocene volcanism occurred.

The Cretaceous unconformity widely recognized on land was observed at Site 439 and could be further extrapolated seaward by the aid of seismic records suggesting that a pre-Oligocene forearc once extended at least to the present midslope terrace where Site 440 is located. The objective at Site 584 was to further confirm and detail the findings of Legs 56 and 57. Site 584, at the outer slope, reached sediment of middle Miocene age, confirming persistent subsidence during the Miocene. It was suggested that extensional tectonics continued from the middle Miocene until the early Pliocene. Numerous ash layer records from all the sites suggest that onshore volcanic activity increased near the end of the late Miocene and continued through the early Pliocene.

Leg 186 was planned to establish borehole geophysical observatories that could monitor the ongoing tectonic processes at two sites (Sites 1150 and 1151) ~25 km north and south of 39°N and slightly eastward of Site 439 in longitude.

TECTONIC AND SEISMIC SETTING

Tectonic Setting

The convergent margin off northern Honshu has developed where lower Cretaceous Pacific ocean crust underthrusts the Eurasian plate in a west-northwest direction. A 9.1-cm/yr convergence rate between these two plates has been estimated (e.g., DeMets et al., 1994). The topographic features of the Japan Trench system consist of a deep-sea terrace, inner trench slope, midslope terrace, trench lower slope, Japan Trench, and outer trench slope (Fig. **F3**). A forearc basin develops in the deep-sea terrace and trench upper slope, which extends from the northwest coast of Hokkaido more than 600 km to the south and is filled with Neogene sediments as much as 5 km thick. Sites 1150 and 1151 on the deep-sea terrace, located ~100 km west of the Japan Trench, are on the eastern edge of the forearc basin, where the Neogene section is ~1.5 km thick (see **"Sedimentation Rates,"** p. 35, in the "Site 1150" chapter and **"Sedimentation Rates,"** p. 23, in the "Site 1151" chapter).

In multichannel seismic profiles, the reflective sequence above a major diffracting horizon represents a seaward transgressive sequence across an extensive angular unconformity (Fig. **F4**). Landward-dipping reflectors below the unconformity may represent formerly accreted sediments or folded and tilted older sedimentary rocks; they are dated by drilling as Upper Cretaceous at Site 439. The Neogene sequence is cut by landward-dipping normal faults spaced ~10 to 15 km apart (Nasu et al., 1980). Seismic refraction measurements indicate a continental crustal velocity structure beneath the deep-sea terrace (Murauchi and Ludwig, 1980; Suyehiro and Nishizawa, 1994).

Tectonic history in the convergent margin near the Japan Trench is characterized by tectonic subsidence and erosion. Regional subsidence during the latest period of plate convergence was established during DSDP drilling along the Japan Trench margin (von Huene, Nasu, et al., 1978) by coring through a subaerial erosion surface many kilometers below sea level (Fig. **F5**). That erosion surface corresponds to an angular unconformity that cuts across tilted beds and is buried beneath subhorizontal strata of the outer shelf and slope. The unconformity extends throughout a 150-km-long area (Nasu et al., 1980; von Huene et al.,

F3. Schematic cross section of the Japan Trench-arc system, p. 21.

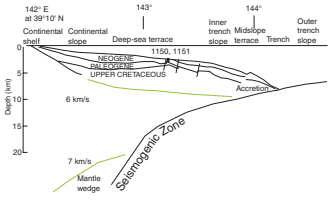

F4. Seismic record section across the Japan Trench, p. 22.

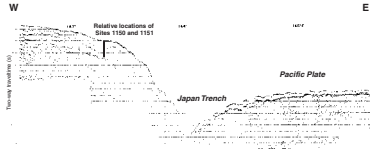

F5. A model of tectonic subsidence history, p. 23.

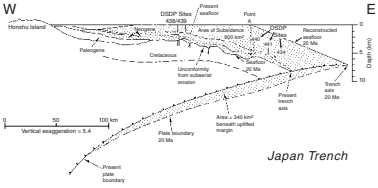

1982) and shows no sign of ending beyond the published seismic coverage. Across the unconformity, seismic velocity increases abruptly from ~1.9 to 4.2 km/s (Murauchi and Ludwig, 1980; Suyehiro and Nishizawa, 1994), consistent with the contact between unconsolidated Oligocene to Quaternary strata and well-consolidated Cretaceous rock as drilled at DSDP Site 439. The sedimentary strata above the unconformity consist of a 48-m-thick breccia and conglomerate of dacite and rhyolite boulders, covered by 50 m of medium-grained sand containing abundant little-transported macrofossils, which was in turn buried by silt and sand turbidites (Scientific Party, 1980) with a probable seaward source (von Huene et al., 1982). The upper 800 m of the section consists of Miocene diatomaceous mud. The regional extent of rock types and erosion was explained by subsidence of a landmass during the past 22 m.y. (Scientific Party, 1980; von Huene et al., 1982). Benthic microfossils from the sediments indicate a succession of water depth consistent with such a history (Arthur et al., 1980; Keller, 1980).

Seismic Setting

In the Japan Trench area, seven large (magnitude [M] = >7) interplate events have occurred in the last 30 yr between 38°N and 41°N. Recent large events are the 1968 Tokachi-Oki earthquake (~41°N; moment magnitude [Mw] = 7.9) and the 28 December 1994 Far-off Sanriku earthquake (~40°N; Mw = 7.7) (Fig. F6). These events, however, are not sufficient to account for the subducting rate of ~8–10 cm/yr. Thus, the seismic coupling seems much smaller along the Japan Trench (35°N–41°N) as compared with the Kurile Trench or Nankai Trough regions, which have a higher seismic energy release rate. Subduction at the Japan Trench may be proceeding by stable sliding either with relatively small (surface-wave magnitude [Ms] = <8) events only or with less frequent large events.

There is a third important category whereby the subduction rate is accommodated by episodic aseismic events of time constants on the order of 10 min to several days (slow earthquakes). Such events, if they exist, are extremely difficult to detect at present. Kawasaki et al. (1995) reported that an ultra-slow earthquake estimated to be Mw 7.3–7.7 accompanied the 1992 Off-Sanriku (39.42°N, 143.33°E; Mw = 6.9) earthquake, based on strain records observed ~120–170 km away from the source. A postseismic strain change of 10^{-7} to 10^{-8} with a time constant of about a day were observed by quartz-tube extensometers (devices that measure linear strain changes). Historically, in the same area, the 1896 Sanriku tsunami earthquake (Mw = ~8.5 but body-wave magnitude [Mb] = ~7) killed ~22,000 people. Tsunami earthquakes rupture with a much longer time constant of minutes compared to the normal type (Tanioka and Satake, 1996).

More recently, the Japanese global positioning system network revealed a postseismic motion of northern Japan after the 1994 Far-off Sanriku earthquake (M = 7.2) that can be explained by a stress diffusion model assuming slow slip on the earthquake fault (Heki et al., 1997). A different, but previously more prevalent interpretation is that the postseismic deformation is a result of aseismic slip at a depth extending below the seismogenic zone.

The above-mentioned large episodic events are responsible for the plate motion. There are numerous microearthquakes, which contribute little to tectonics but delineate the characteristics of seismogenic zone (Fig. F7). Microearthquake activity in this area shows spatially clustered

F6. Epicenters of large thrust earthquakes, p. 24.

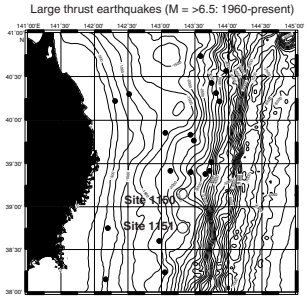

F7. Map of Japan Trench area with seismicity, p. 25.

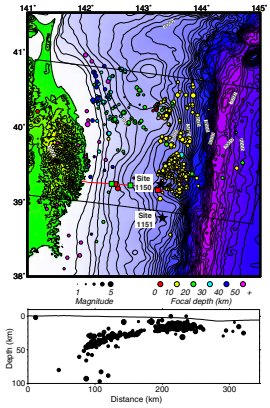

occurrence over at least a few tens of years. The plate geometry from microearthquakes suggests that a large bend occurs at ~20 km depth. The seismic activity seems to have a gap above and below this depth along the plate boundary. The shallower activity is conspicuously high between 39°N–41°N.

The seismic velocity structure of this area is characterized by a small accretionary wedge (Fig. F3). High velocity (> 6 km/s) material reaches beneath the inner trench slope. Either an extension of the island arc lower crust or the mantle wedge seems to meet the plate boundary where it plunges. Large thrust earthquakes in this area often initiate from the updip end of the seismogenic zone and reach beneath the coastline. It can be seen from detailed velocity structure models that there is no obvious correlation with the updip and downdip ends. This suggests that the key factors controlling the seismic activity are not in bulk properties, but rather in the localized properties at the well-developed décollement.

OPERATIONS STRATEGY

Previous drilling in the Japan Trench region was in the DSDP era before the advent of advanced hydraulic piston corer/extended core barrel (APC/XCB) technology (Legs 56 and 57 in 1977 and Leg 87 in 1982). Previous ODP drilling at plate subduction zones were at Izu-Marianas, Barbados, Costa Rica, Cascadia, Nankai, and Peru margins, which span quite different subduction types. Both Sites 1150 and 1151 are located at the deep-sea terrace at 2681- and 2182-m water depths, respectively (Table T1).

T1. Leg 186 operational summary, p. 37.

A unique aspect of Leg 186 was the installation of two permanent borehole geophysical observatories. The installation required complex operations that had never before been done. In this region, a clear deep-seismic reflector is the Cretaceous unconformity, below which the physical properties such as *P*-wave velocities and densities become more favorable for the sensors. However, it did not seem feasible to drill to depths of >1.5 s in two-way traveltime at the two sites to penetrate the Cretaceous unconformity. Such an operation would have required an interim supply of casing joints during the leg and considerably more time than available on a standard leg. Therefore, a provisional depth of 1000 m was targeted for rotary core barrel (RCB) coring and to check if the physical properties values were acceptable for the instruments. Logging data and observations from cores allowed us to monitor physical properties and decide on a suitable depth.

For initial coring objectives, one site with a fast sedimentation rate was to be double APC/XCB cored to ensure complete recovery in the Pliocene and younger section. Because of large uncertainties in installation time requirements, double APC coring was postponed until Site 1151.

Each site was equipped with a reentry cone and was cased through unstable sections leaving a 50- to 100-m open-hole section at the bottom. Because the sensor package diameter cannot run through the drill string as logging tools do, it had to be connected at the bottom of the drill string. To cement in the sensors, which is essential for the strain measurements, the drillship was required.

At Site 1150, the original plan for XCB coring to 450 mbsf level was deepened to 723 mbsf. Hole 1150B was thus drilled to 703 mbsf and cored to 1182 mbsf. Below ~1100 mbsf, the physical properties seemed

to be adequate for the instrument. Logging data further confirmed and pinpointed what the instrument depth should be. The unfortunate abandonment of reentry Hole 1150C because of probable defects in the reentry cone caused a major change of plans. We had to go back to the port of Yokohama to obtain another reentry cone, at which time we also loaded the remaining 4½-in casing pipes purchased for hanging the instrument package in the drilled and cased holes. At this point, we focused the use of time on accomplishing the primary objectives for the leg, which meant that many other objectives might have to be temporarily abandoned.

The Site 1150 installation was successfully completed at 1900 hr on 28 July, with only 18 days left for operations at the second site. It was then that we decided to skip APC/XCB coring and logging and instead aim for the shortest pathway to complete the observatory installation. Thus, Hole 1151A was RCB cored all the way to 1114 mbsf. The operations at Hole 1151B proceeded rapidly, and we successfully completed the instrument installation on 9 August, just 12 days after arriving on site. After the installation, we proceeded to complete the remaining objectives for the hole, which included double APC coring this site to ~100 mbsf, and then logging to 870 mbsf.

SCIENTIFIC OBJECTIVES

The Leg 186 Scientific Party sailed out to investigate the dynamic properties of one of the world's most active plate subduction zones, the Japan Trench, where the oldest oceanic plate (>100 Ma) is subducting at a high rate (~90 km/m.y.). The drill sites were located about midway within the Japan Trench zone, which is ~650 km long.

The prime objective of this leg was to establish two geophysical observatories that monitor strain, tilt, and seismic waves to further our understanding of subduction dynamics. Coring and logging were aimed at gathering information about past and present tectonic and paleoceanographic conditions.

Dynamic Sliding of the Subducting Plate and Earthquake Process

The seismic coupling efficiency of the subduction zone off Tohoku appears to be as low as 25%. This means that of the total Pacific plate motion expected, only one-quarter is seen as stick-slip motion leading to thrust-type earthquakes. One possibility is that three-quarters of the motion is released as slow earthquakes, which are not recorded on normal seismographs. In the past, sparse observations suggest that the slow strain release may consist of multiple episodes in which each event is rather small. For this reason, installation of an instrument of the highest achievable sensitivity is required. Any data leading to better understanding of the partitioning of strain release into damaging "fast" events and slower events will be extremely valuable and may lend further insight into the whole earthquake process.

The plate boundary off northeast Japan fulfills three important conditions for a long-term geophysical observatory:

1. Dense geophysical networks already exist on land to optimally link to our observatories installed during Leg 186.

2. Moderately large (M = ~7) seismic events occur frequently, and aseismic slips (slow earthquakes) with comparable or larger magnitude are expected to occur even more frequently.
3. Crustal and uppermost mantle structures have been well studied by reflection-refraction seismic surveys (Suyehiro et al., 1985a, 1985b, 1990; Suyehiro and Nishizawa, 1994).

Earthquake Source Studies

Generally, interplate thrust earthquakes occur within a zone termed the seismogenic zone. The definition and controlling factors of this zone, however, are unclear. Temperature, material, or pore pressure that affect the frictional state of the fault are consequences of geological processes. But their relationship is unclear. We need to define what a seismogenic zone is, if we are to relate to physical properties of the interacting plates. It is critically important to know exactly where earthquakes of various sizes are occurring. At present, it is not possible to locate earthquake faults using seismic techniques with less than several hundred meters' accuracy relative to where the faults and velocity heterogeneities are. Where a local seismic network does not exist, the accuracy is often much worse and can be more than several kilometers in error.

The borehole geophysical observatories at Sites 1150 and 1151 will greatly improve source location (particularly depth) and focal mechanism and rupture process determinations of the earthquakes near the Japan Trench (Nishizawa et al., 1990, 1992; Suyehiro and Nishizawa, 1994; Hino et al., 1996). Near-field data, obtained from these observatories with the aid of ocean bottom seismographs, will particularly improve the resolution of source mechanisms of very slow rupture events such as tsunami earthquakes. These earthquakes may occur seaward of the updip end of normal thrust earthquakes (e.g., Tanioka and Satake, 1996).

High-Resolution Geometry of the Plate Boundary

The two stations at Sites 1150 and 1151 will be linked to the network of broadband and/or very broadband seismometers on the main Japanese islands and will make a dense seismic network that is 50 km in scale. The observations of various phases of body waves from the many shallow to deep earthquakes within the network will provide sufficient data to improve the structural image of the plate boundary—in particular, the changes in physical properties associated with tectonic erosion and seismogenesis.

Miocene and Younger Volcanic Ash Stratigraphy in the Western Pacific

The cores represent an important reference section near Japan to compare with the remote ash deposits already cored to the east. They will also provide important information about eruptive processes, volcanic hazards, and aspects of climate such as response to wind, sand, and volcanogenic input of greenhouse and related gases (J. Natland, pers. comm., 1997).

During Leg 132, a number of rhyolitic to dacitic volcanic ash beds were recovered on Shatsky Rise, east of Japan. Comparison with ash stratigraphy at DSDP Sites 578–580, about halfway between Shatsky

Rise and Japan, indicates that the Shatsky ash beds were derived either from Japan or the Kurile-Kamchatka arc systems and that they were carried far to the east on the high-speed polar and subtropical jet streams (Natland, 1993). A summary appraisal is that 25–40 eruptions in the past 3 m.y. produced ash that reached one or more of those sites, with ~10% of these reaching Shatsky Rise in the form of discrete ash beds or pumice. Some of the eruptions were extremely large, resulting in deposits 5 to 15 cm thick, even on Shatsky Rise. The last drilling in this region was during DSDP Legs 56 and 57, before the advent of hydraulic piston coring. An important, although seriously incomplete and at times highly disturbed, ash record was recovered in Holes 438A and 440B (e.g., Cadet and Fujioka, 1980).

Subsidence History Across the Continental Slope to Constrain the Processes of Tectonic Erosion

Quantitative estimates of the tectonic erosion process were made for the Neogene history of the Japan Trench region based on drilling and seismic records (von Huene and Lallemand, 1990; von Huene et al., 1994). Key evidence came from DSDP Site 439. Evidence collected from additional coring at ODP Sites 1150 and 1151, which are ~200 km south of Site 439, will further constrain the timing and erosion volumes in relation to backarc opening and the style of convergence. The comparison of results between 38°N and 41°N will delineate relative changes along the axis.

SITE 1150

Site 1150 is located in the deep-sea terrace on the landward side of the Japan Trench. The primary objective was to establish a borehole geophysical observatory to monitor seismo-geodetic signals immediately above the active portion of the seismogenic zone where large interplate thrust earthquakes recur. The first successful emplacement of a borehole geophysical observatory (NEREID-1) with a three-component strainmeter, a two-component tiltmeter, and three-component broadband seismometers was completed on 28 July. The sensing sections are <11 m in length bottoming at 1120 mbsf and were cemented in the 105-m-long open hole at Hole 1150D. Because the instrument string and battery frame could not be installed simultaneously, the electrical connection to the downhole instruments was made after Leg 186. The observatory sites were visited by the *Dolphin 3K* of the Japan Marine Science and Technology Center (JAMSTEC) between 2 and 10 September to start the systems, check the status, and collect initial data. The observatories are designed to be serviced at least once a year.

All of the cores from 0 to 722.6 mbsf from Hole 1150A are dominated by diatomaceous silty clay. The upper 200 m of sediment consists of interbedded diatomaceous ooze and clay, with common siliceous biogenic grains, diatoms, radiolarians, and sponge spicules and rare foraminifers and nannofossils. Volcanic glass and siliciclastic grains are also observed in smear slides, though they compose <10% of the total sediment. From 260 to ~620 mbsf, the sediments gradually become firmer and more hemipelagic with increasing depth. Compared with cores from the upper 200 m, volcanic ash, reworked ash layers, volcanic pebbles, thin turbiditic sand, and silt layers are rare but present in the lower section. Below ~620 mbsf, cores from both Hole 1150A (620–722

mbsf) and Hole 1150B (703–1181.6 mbsf) consist mainly of well-lithified diatomaceous silty claystone. Authigenic glauconitic sand is interbedded with the dominant clayey lithology below 430 mbsf in Hole 1150A and from the start of the cored interval (703 mbsf) at Hole 1150B. Local occurrences of detrital glauconite in minor amounts are rare within both holes. Bioturbation (*Chondrites, Zoophycos,* and *Planolites*) is abundant in Hole 1150B. A few carbonaceous layers and nodule-type accumulations are also found interbedded in the largely homogeneous diatomaceous silty claystone in Hole 1150B. Volcanic ash layers are rare in this hole.

Twelve diatom zonations were identified from core-catcher samples from Holes 1150A and 1150B. The age of the lowermost sediment is interpreted to be younger than 9.9 Ma because the first occurrence of *Denticulopsis dimorpha* was not observed in the studied interval. The average sedimentation rate is 119 m/m.y., with higher sedimentation rates (>200 m/m.y.) occurring between 6.65–3.74 Ma and between 0.3 and 0.0 Ma. The lowest sedimentation rate occurs between 2.0 and ~1.24 Ma (18 m/m.y.). The Pliocene/Pleistocene boundary lies at ~110 mbsf, and the Pliocene/Miocene boundary is at ~500 mbsf. Datums of calcareous nannofossils were difficult to determine accurately because of poor preservation and a low abundance of these fossils. Of the 11 nannofossil datums identified, seven gave ages younger than those indicated by the diatom datums.

Chemical analyses of pore waters from Hole 1150A cores show that chlorinity gradually decreases with depth from ~550 mM at the top of the hole to 500 mM at ~200 mbsf. Chlorinity concentrations remain at about this value for 350 m downhole. From ~550 mbsf, values abruptly decrease with depth to reach a minimum of 350 mM at ~700 mbsf. A similar trend is observed in the magnesium, potassium, and alkalinity profiles. Values gradually decrease in the upper 200 m (from ~50 to 28 mM for magnesium; from ~11 to 8 mM for potassium; and from ~50 to 26 mM for alkalinity). Values remain fairly constant from ~200 to 500 mbsf and drastically decrease with depth to reach minimum values of 11 mM for magnesium, 6 mM for potassium, and 11 mM for alkalinity. Calcium concentrations increase from ~2 to 8 mM in the upper 200 m, remain fairly constant to a depth of 400 mbsf, and then increase to 10 mM at 600 mbsf.

Bulk-elemental analyses for the upper 350 m of samples from Hole 1150A show relatively high concentrations of organic carbon. Values fluctuate with depth between 1.8 and 0.5 wt%. Typical values are ~1 wt%. Sulfur abundances also are relatively high in this interval. Typical values are ~0.9 wt%, fluctuating between 1.3 and 0.5 wt%. Nitrogen abundances are typically ~0.13 wt%, fluctuating between 0.6 and 0.1 wt%.

Gas analyses for Hole 1150B indicate that methane concentrations are between 2% and 8% as measured from headspace gas analysis. Ethane concentrations are typically ~6 ppm from 700 to 900 mbsf. Values then slightly increase with depth to typical values of ~14 ppm. Methane/ethane ratios tend to decrease gradually with depth from ~5000 at 700 mbsf to 2800 at the final depth of ~1200 mbsf. Other hydrocarbon gases are below the detection limits.

Physical properties data show several systematic trends that correlate with downhole chemical and lithologic changes, appearing to indicate variations in hydrological and mechanical conditions. Gas expansion and drilling disturbance (formation of drilling biscuits) affect the physical properties of most cores from Hole 1150A. The interval from the

mudline to 222 mbsf consists of hemipelagic diatomaceous ooze and clay. Inverse trends in index properties are observed from ~113 to ~200 mbsf. Bulk density decreases from ~1.7 to 1.3 g/cm^3, and porosity increases from ~56% to 79%. Constant to slightly inverse trends with uniform values of index properties are observed from ~200 to 600 mbsf. The top of this interval coincides with a small change in lithologic composition, whereas the bottom corresponds to the change from firm sediments to sedimentary rocks. Bulk density and porosity range from ~1.3 to 1.6 g/cm^3 and 63% to 77%, respectively.

Because of scattering and attenuation of the signal in the sediment, *P*-wave velocity was only measured sporadically above 304 mbsf. The horizontal velocity drops to >1.50 km/s below 750 mbsf, which is followed by a generally increasing trend to >1.90 km/s at the base of Hole 1150B. Vertical *P*-wave velocity was measured from below 710 mbsf and is generally somewhat lower than horizontal *P*-wave velocity. Horizontal *P*-wave velocity gradually increases downhole from 1.45 km/s at 304 mbsf to 1.95 km/s at 710 mbsf. There may be a bias in index properties and *P*-wave velocity measurements in this interval because only coherent and undisturbed pieces were sampled. Measurements in sedimentary rocks show a wide scatter in porosity, bulk density, and *P*-wave velocity but suggest generally decreasing porosity and increasing bulk density and *P*-wave velocity trends. Preliminary analyses of sonic anisotropy combined with paleomagnetic declination data indicate that the sedimentary rock from 730 to 1180 mbsf is anisotropic, with maximum, intermediate, and minimum principal axes along the west-northwest to east-southeast, north-northwest to south-southwest, and vertical orientations, respectively. In the interval where the borehole instruments were installed, the porosity, bulk density, and *P*-wave velocity are 55%, 1.65 g/cm^3, and 2.0 km/s, respectively.

The magnetization of the first eight cores has an unambiguous normal polarity direction, with a steep downward inclination and a northward declination after applying the Tensor-tool orientation correction. The Brunhes/Matuyama boundary is most likely located in Core 186-1150A-10H at ~84–88 mbsf, though coring disturbance makes interpretation tenuous in this interval. Above 850 mbsf, the position of several reversals are evident following alternating-field demagnetization. These should be useful in establishing a few magnetostratigraphic tie points in the Pliocene–Miocene section at this site. The magnetization of the RCB cores from Hole 1150B is fairly stable, and polarity is dominantly normal below 850 mbsf. The declinations from the Hole 1150B cores have proved useful for reconstructing structural orientations of the numerous microfaults and fractures observed in the core. For example, after reorienting fracture and fault planes into geographic coordinates, we find that most in the depth range from 703 to 940 have north-south strikes and dips of 45° to 80°, with a clear preference for eastward-dipping planes. Normal offset is observed on most of the fault planes, suggesting that an east-west extensional stress field is responsible for the deformation observed in this interval. The extensional stress direction changes downhole, so that below 1080 mbsf the dominant direction is west-northwest to east-southeast.

Equilibrium temperatures obtained from the APC temperature tool (Adara) and the Davis-Villinger temperature probe in the interval from 0 to 154.8 mbsf give a geothermal gradient of 28.9°C/km. The calculated heat flow is 20.1 mW/m^2, which, though low relative to global values, is typical for the tectonic environment.

Three logging tool combinations were used in Hole 1150B: the triple combination tool string, the Formation MicroScanner (FMS)/digital sonic tool string, and the borehole televiewer tool string.

Although operational difficulties prevented logging at ~650 mbsf, three strings were deployed down to ~1170 mbsf after a wiper trip operation. Data quality is good throughout the logged intervals. The whole logged section can be divided into six units using the resistivity log in conjunction with other logs. These units are consistent with core descriptions and core measurements. The FMS data show borehole geometries to be oval below ~750 mbsf with east-west elongation (20 cm in north-south and 30–35 cm in east-west). The in situ physical properties values in the lowermost 100 m (i.e., in the interval where the borehole instruments were installed) are ~1.95 km/s for *P*-wave velocity, ~1.7 g/cm^3 for bulk density, 55%–60% for porosity, 1.2 Ωm for resistivity, and ~50 cps for spectral natural gamma ray.

SITE 1151

Site 1151 is located 48 km south of Site 1150, in the deep-sea terrace of the Japan Trench, a similar geological setting as at Site 1150. The main objective at this site was to establish another borehole geophysical observatory to monitor active processes in a plate subduction zone with strain, tilt, and seismic sensors. A key difference is that this area is above an aseismic portion of the seismogenic zone. The strainmeter at this site measures volumetric strain changes. This second seafloor borehole geophysical observatory (NEREID-2) was successfully installed in Hole 1151B with much less downtime than for the first one. The sensor string was set in a section with a density of ~1.9 g/cm^3 and *P*-wave velocity of ~2000 m/s. The target depth is slightly shallower at 1095 mbsf for the sensor string bottom, but the physical properties data suggest a more competent rock environment than at Site 1150. The bottom of the open hole was filled with cement up to ~50 m into the cased hole section. The observatory sites were visited by the *Dolphin 3K* of JAMSTEC between 2 and 10 September to start and check the system.

At Site 1151, the sedimentary section from 0 to 1113 mbsf was cored with APC (Holes 1151C and 1151D) and RCB (Hole 1151A) coring systems. The recovered sequence ranges from Holocene to middle Miocene age. The average recovery was 68% for Hole 1151A and ~100% for Holes 1151C and 1151D. The common major lithology at this site is diatomaceous silty clay with intercalations of minor lithologies such as volcaniclastic ash, pumice, silt, and sand. Brittle deformational structures dominate below 400 mbsf. Bioturbation can be seen in most cores below 300 mbsf. Detrital glauconite occurs as sand-sized grains distributed throughout the section. Authigenic glauconite, found in both the major and minor lithologies, is of fine silt size. The detrital glauconite is always found in association with the finer grained authigenic glauconite, but the latter may occur in the absence of the former. Alteration to limonite locally occurs. The following lithologic units were identified:

Unit I (0–295 mbsf; 0–4.5 Ma) consists of diatomaceous silty clay. Minor lithologies (sand, silt, ash, and pumice) occur frequently except in the range 78–106 mbsf. The biogenic components increase to their peak value.

Unit II (295–411 mbsf; 4.5–5.5 Ma) consists of diatomaceous spicule-bearing silty clay. Ash and pumice are rare throughout the unit.

Unit III (411–817 mbsf; 5.5–7.5 Ma) consists of various combinations of diatom-, glass-, and spicule-bearing silty clay. Brittle deformational structures occur first and reach their peak within this unit. Siliciclastic components compose >50% of the sediments.

Unit IV (817–1007 mbsf; 7.5–11.5 Ma) consists of diatom- and spicule-bearing claystone. Minor lithologies are rare. Unit V (1007–1113 mbsf; 11.5–16 Ma) consists of combinations of glassy or glass-bearing silty claystone, locally spicule bearing. The diatoms compose <10% of the sediment.

As at Site 1150, diatom datums provide the main age constraints, with diatoms being few to abundant throughout the sequence, except for some ash and dolomite layers. Overall, we identified 24 diatom datums from core-catcher samples, with the lowest being in the middle Miocene (<16.3 Ma). Diatom assemblages from all samples consist almost entirely of oceanic species, mainly from the subarctic North Pacific Ocean. Calcareous nannofossils are generally barren to abundant, with variable preservation. Similar to Site 1150, we identified 11 nannofossil datums, and seven of these gave ages younger than indicated by the diatom datums.

Sedimentation rates at Site 1151 were estimated using a combination of biostratigraphy and magnetostratigraphy. The upper 200 m has a relatively low rate (20 to 152 m/m.y.). It increases between 200 and 450 mbsf, reaching ~240 m/m.y., and remains at that level down to 800 mbsf, below which the rate gradually decreases. At 1027 mbsf, there is a hiatus of >0.2 m.y., and the rate then gradually increases downhole to 43 m/m.y. Site 1151 had high rates in the latest Miocene and low rates before and after this, a pattern similar to that at Site 1150. The intervals of low rate correspond to the early late Miocene (before 8.5 Ma) and the early to mid-Pleistocene (2.0–0.78 Ma).

Gas analyses at Site 1151 indicate that methane concentrations are between 0.4% to 5% with an average concentration of ~2%. Ethane concentrations fluctuate between 1 and 12 ppmv and typically are of ~4 ppmv. Methane/ethane ratios are ~4400 throughout. Other hydrocarbon gases are below the detection limit.

No trend is present in the distribution of carbonate abundances with depth. Abundances range from 0.08 to 79 wt%, with an average value of 3.3 wt%. Most values, however fall between 2 and 4 wt%, with excursions having peak values as high as 15 wt%. Low carbonate abundances are in agreement with low occurrences of calcareous fossils in the sediments.

Sediments exhibit relatively high abundances of organic matter with characteristic low (<10) C/N ratios. Abundance of organic carbon (C_{org}) fluctuates between 0.2 and 1.4 wt%, with an average value of ~0.9 wt%. Total sulfur abundances irregularly fluctuate between 0.35 to 1.5 wt%, with an average value of 0.85 wt%.

Several geochemical parameters exhibit similar distributions with depth. K^+, Na^+, Mg^{2+}, chlorinity, and salinity show a characteristic decreasing trend with depth. Salinity gradually decreases with depth from a value of ~32 at the top of the borehole to a value of 18 at ~900 mbsf. Below this depth, salinity remains constant at 18 to the final depth. Chlorinity concentrations remain constant at ~500 mM in the upper 200 m of the borehole and then steadily decrease to 320 mM at the final depth.

Alkalinity values gradually decrease downhole in the upper 200 m from 31 to 17 mM and then increase to 25 mM at ~450 mbsf. Below

this depth, values decrease steadily downhole to 2 mM at the bottom. Dissolved sulfate concentrations exhibit values lower than 2 mM throughout.

Concentrations of dissolved calcium (Ca^{2+}) in pore waters slightly increase downhole from ~3 mM at the top to 18 mM at the bottom. Concentrations of dissolved strontium (Sr^{2+}) fluctuate between 100 and 130 µM down to 550 mbsf and then increase to reach a maximum value of 232 µM at the bottom. Concentrations of dissolved lithium (Li^{+}) gradually increase from 20 to 480 µM in the upper 850 m and then decrease to ~280 µM at the bottom.

The gamma-ray attenuation bulk density in Hole 1151A ranges from ~1.3 to 2.0 g/cm³. Lithologic Unit II is characterized by rather constant values, averaging ~1.4 g/cm³. Density varies from 1.3 to 1.7 g/cm³ along an oscillating trend in Unit III. Similar oscillating trends increase in magnitude in Units IV (1.3–1.8 g/cm³) and V (1.4–2.0 g/cm³). Such an oscillating trend is also observed in natural gamma-ray activity. The average thermal gradient, which was obtained from three measurements, is 35.9°C/km.

In Hole 1151A, *P*-wave velocity (horizontal) ranges from 1540 to 5290 m/s, with most values being <2150 m/s. The highest velocities were measured in thin beds of carbonate-rich sediments (i.e., dolomite layers or dolomite concretions). The maximum velocity in Hole 1151A of 5290 m/s was measured on a dolomite concretion at 1108 mbsf.

The ranges of porosity, bulk density, and grain density in Hole 1151A are 10%–77%, 1.32 to 2.42 g/cm³, and 2.09 to 3.91 g/cm³, respectively. The section from 78 to 295 mbsf (Unit I) has scattered, but slightly inverse trends of porosity and bulk density: porosity and bulk density generally range from 57% to 77% and from 1.32 to 1.59 g/cm³, respectively. The top of Unit IV (825 mbsf) coincides with a shift to higher porosity and lower bulk density values. Yet another significant shift to higher porosity, by ~13%, occurs from 963 to 977 mbsf. The corresponding decrease in bulk density is ~0.22 g/cm³. Apart from these two shifts, index properties show normal trends across Units IV and V. At the base of Hole 1151A, porosity, bulk density and grain density are 49%, 1.75 g/cm³, and 2.46 g/cm³, respectively.

The remanent magnetization at Site 1151 is very similar in behavior to that at Site 1150. The upper 78 m has an unambiguous normal polarity direction, with a steep downward inclination. The location of the Brunhes/Matuyama reversal appears to be well resolved by the abrupt downhole change to negative inclinations at ~78.2 mbsf in Hole 1151C, 80.1 mbsf in Hole 1151D, and 82–84 mbsf (between Cores 186-1151A-2R and 3R) in Hole 1151A. However, the reversals lower in the section are not easily correlated with the geomagnetic polarity time scale. Below 700 m, virtually the entire section has very stable positive inclinations that average ~60°. We interpret this interval to be partially or totally overprinted by a recent normal polarity field direction. The stable declinations from these cores have proved useful for reconstructing structural orientations of the microfractures and bedding planes. We have found that the orientation of fracture planes changes downhole with dip azimuths dominantly to the west-northeast and east-southeast in the upper domain but dominantly east and west in the middle and lower domains. Below 900 mbsf, the dip angles of bedding planes are >10° and preferentially dip toward the east.

Three logging runs (one triple combo and two FMS/sonic runs down to 850 mbsf) were achieved in Hole 1151D by extending the second

APC/XCB hole. The hole condition (caliper log) was much more stable at Site 1151, and logging was accomplished without difficulty.

ACCOMPLISHMENTS AND INTERESTING OBSERVATIONS

The principal objective of Leg 186 was to install two permanent borehole observatories with several seismic and deformation-measuring sensors. A strainmeter, tiltmeter, and two broad-frequency range seismometers were grouted in at the bottom of boreholes drilled deep enough to penetrate higher velocity, indurated rock. This objective was successfully achieved. Figures **F8** and **F9** show the seafloor installation as well as the arrangement of sensors in the borehole. Actual vibration-isolated television camera views of the seafloor unit are shown in Figure **F10.** In addition, both sites were cored to instrument depth and have yielded scientific results of considerable interest. In all, we recovered 1742 m of core from the two sites, despite the major emphasis on instrument installation. The dominant lithology was diatomaceous silty clay or claystone with many ash and some dolomite layers (Fig. **F11**).

Compared with results from earlier drilling along the Japan Trench, the salinity and chlorinity variations with depth exhibit both similar behavior and significant differences. Sites along the deep-sea terrace—Sites 1150, 1151, 438, and 439—have chlorinity of 550–550 mM just below the seafloor, decreasing to ~300 mM at a depth of 1000 m. In contrast, sites far from the subducting slab, such as the ODP Legs 127 and 128 Sea of Japan Sites 798 and 799, and sites near the trench (Site 536) have chlorinity that does not decrease as much. Figure **F12** shows a comparison of the deep-sea terrace data from Sites 1150, 1151, and 438, and data from the Sea of Japan Site 799. Site 1150 has a notable deviation from the monotonic behavior of other sites. Down to 600 m the chlorinity does not drop below 500 mM, but below 650 m, the values drop to those of the other terrace sites. One tentative explanation is that in the terrace sites, there is a supply of freshwater from depth that mixes (possibly continuously) with the saline sea bottom–derived water. In Site 1150, a less permeable layer interrupts this mixing so that the upper part is isolated from freshwater. In other areas such as the Sea of Japan sites or the near trench sites, this freshwater supply is not available. A possible source of the freshwater is dehydration of slab interface components at depth where earthquakes occur (i.e., deeper than 10 km).

The age of the sediments of Sites 1150 and 1151, as well as those from Sites 438 and 584 farther to the north, are shown in Figure **F13.** The sedimentation rates derived from these data are shown in Figure **F14.** Aside from the generally lower rate of sedimentation from 0.5–3 Ma or so, a notable feature is the fairly widespread increase at 6–8 Ma. Many factors can be responsible for this increase and one of the important contributions of Leg 186 is to provide the samples and data that can be used postcruise to constrain these possibilities. The tantalizing range of causes include change in wind direction or increase in the rate of mountain building because of increased tectonic compression.

There have been major changes in the tectonics of Japan. Until 14 m.y. ago, the islands were subjected to east-west tension, and the Sea of Japan was opening. Today, there is strong east-west compression. It is possible that some of the change in sediment flux as well as volcanic

F8. Schematic of the seafloor and borehole installation for Hole 1150D, p. 26.

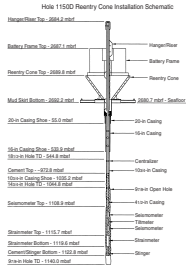

F9. Schematic of the seafloor and borehole installation for Hole 1151B, p. 27.

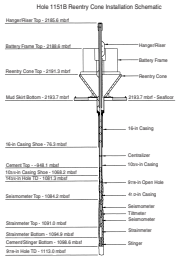

F10. The successfully deployed battery pack, p. 28.

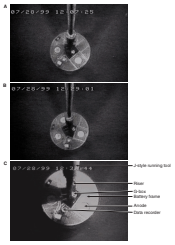

F11. Lithostratigraphic summary, p. 29.

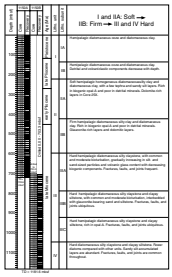

output is affected by the changes in the force system at the subduction interface. From Figure **F15** it is apparent that there was a major increase in volcanic deposits at Site 1150 at ~3 Ma and a decrease in the most recent half a million years or so. At Site 1151, the increase starts at ~4 Ma. Further north (40.6°N) in Hole 438A, volcanism increased from ~5 Ma until ~2 Ma. The cores collected during Leg 186 will enable us to identify, quantify, and date the ash layers derived from great volcanic eruptions.

Whereas a major goal of Leg 186 is measuring the current deformation resulting from the subduction forces, the fractures and hole deformation data also bear on that problem. The logging of Hole 1150B indicates significant enlargement of the hole by 40% in the east-west direction. This means that the north-south compressive stresses are greater. This is not surprising because the bending of the upper plate caused by the subduction drag would indeed result in east-west tension in the upper layer. The faults observed in the cores from Hole 1150B are consistent with such an east-west tensional stress field (Fig. **F16A**). Hole 1151D was logged to depths less than 870 m. To that depth there were negligible breakouts, indicating that either stresses are much lower or the rock was much stronger. It is known that the rock at Site 1151 was more stable during drilling than that at Site 1150, but it is not clear what effect is dominant in governing the hole elongation. In addition, Figure **F16B** shows that the fracture directions are less well organized than those of Site 1150. Figure **F17** shows a comparison of the dominantly normal faults in the two holes. The fault density is rather similar, though Site 1150 does have more fractures. Overall, the long-term deformation, as determined by number, orientation, and offset of faults, indicates that the two sites are broadly comparable (Figs. **F16, F17**). Normal faulting dominates in both holes with the extension direction being west-northwest–east-southeast in both cases. Interpreting the differences will be aided by postcruise analysis of the mechanical properties of the cores. In all the above fields and others not mentioned, postcruise analysis of the data and samples provided by Leg 186 will improve our understanding of the processes in this subduction zone.

F12. Chlorinity change in interstitial water, p. 31.

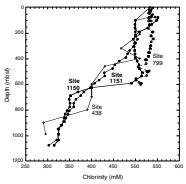

F13. Age-depth curves for Leg 186 sites and other Japan Trench sites, p. 32.

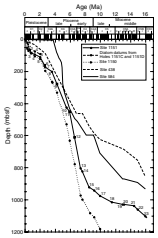

F14. Smoothed curve presentation of sedimentation rates along the Japan Trench, p. 33.

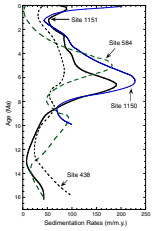

F15. Ash records from Leg 186 compared with other Japan Trench sites, p. 34.

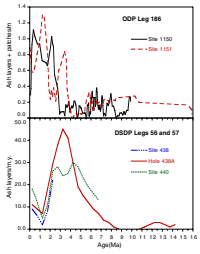

F16. Fault orientations, p. 35.

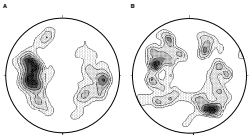

F17. Frequency of faults, p. 36.

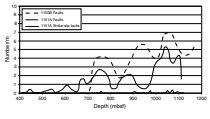

REFERENCES

Arthur, M.A., von Huene, R., and Adelseck, C.G., Jr., 1980. Sedimentary evolution of the Japan fore-arc region off northern Honshu, Legs 56 and 57, Deep Sea Drilling Project. *In* Scientific Party, *Init. Repts. DSDP,* 56, 57 (Pt. 1): Washington (U.S. Govt. Printing Office), 521–568.

BOREHOLE, 1994. BOREHOLE: a plan to advance post-drilling sub-seafloor science. *JOI/USSAC Workshop Rep.,* Univ. Miami, Miami, FL, 1–83.

Cadet, J.-P., and Fujioka, K., 1980. Neogene volcanic ashes and explosive volcanism: Japan Trench transect, Leg 57, Deep Sea Drilling Project. *In* Scientific Party, *Init. Repts. DSDP,* 56, 57 (Pt. 2): Washington (U.S. Govt. Printing Office), 1027–1041.

COSOD II, 1987. *Rep. 2nd Conf. Scientific Ocean Drilling:* Washington/Strasbourg (JOIDES/European Sci. Found.).

DeMets, C., Gordon, R.G., Argus, D.F., and Stein, S., 1994. Effect of recent revisions to the geomagnetic time scale on estimates of current plate motion. *Geophys. Res. Lett.,* 21:2191–2194.

Fukao, Y., 1992. Seismic tomogram of the Earth's mantle: geodynamic implications. *Science,* 258:625–630.

Heki, K., Miyazaki, S., and Tsuji, H., 1997. Silent fault slip following an interplate thrust earthquake at the Japan Trench. *Nature,* 386:595–598.

Hino, R., Kanazawa, T., and Hasegawa, A., 1996. Interplate seismic activity near the northern Japan Trench deduced from ocean bottom and lan

based seismic observations. *Phys. Earth Planet. Inter.,* 93:37–52.

Kagami, H., Karig, D.E., Coulbourn, W.T., et al., 1986. *Init. Repts. DSDP,* 87: Washington (U.S. Govt. Printing Office).

Kawasaki, I., Arai, Y., Tamura, Y., Sagiya, T., Mikami, N., Okada, Y., Sakata, M., and Kasahara, M., 1995. The 1992 Sanriku-Oki, Japan, ultra-slow earthquake. *J. Phys. Earth,* 43:105–116.

Keller, G., 1980. Benthic foraminifers and paleobathymetry of the Japan Trench area, Leg 57, Deep Sea Drilling Project. *In* Scientific Party, *Init. Repts. DSDP,* 56, 57 (Pt. 2): Washington (U.S. Govt. Printing Office), 835–865.

Montagner, J.-P., and Lancelot, Y. (Eds.), 1995. Multidisciplinary observatories on the deep seafloor. *INSU/CNRS, IFREMER, ODP-France, OSN/USSAC, ODP-Japan.*

Murauchi, S., and Ludwig, W.J., 1980. Crustal structure of the Japan Trench: the effect of subduction of ocean crust. *In* Scientific Party, *Init. Repts. DSDP,* 56, 57 (Pt. 1): Washington (U.S. Govt. Printing Office), 463–469.

Nasu, N., von Huene, R., Ishiwada, Y., Langseth, M., Bruns, T., and Honza, E., 1980. Interpretation of multichannel seismic reflection data, Legs 56 and 57, Japan Trench transect, Deep Sea Drilling Project. *In* Scientific Party, *Init. Repts. DSDP,* 56, 57 (Part 1): Washington (U.S. Govt. Printing Office), 489–503.

Natland, J.H., 1993. Volcanic ash and pumice at Shatsky Rise: sources, mechanisms of transport, and bearing on atmospheric circulation. *In* Natland, J.H., Storms, M.A., et al., *Proc. ODP, Sci. Results,* 132: College Station, TX (Ocean Drilling Program), 57–66.

Nishizawa, A., Kanazawa, T., Iwasaki, T., and Shimamura, H., 1992. Spatial distribution of earthquakes associated with the Pacific plate subduction off northeastern Japan revealed by ocean bottom and land observation. *Phys. Earth Planet. Inter.,* 75:165–175.

Nishizawa, A., Kono, T., Hasegawa, A., Hirasawa, T., Kanazawa, T., and Iwasaki, T., 1990. Spatial distribution of earthquakes off Sanriku, Northeastern Japan, in 1989 determined by ocean-bottom and land-based observation. *J. Phys. Earth,* 38:347–360.

Ocean Drilling Program, 1996. *Understanding Our Dynamic Earth through Ocean Drilling: Ocean Drilling Program Long Range Plan Into the 21st Century:* Washington (Joint Oceanographic Institutions).

Purdy, G.M., and Dziewonski, A.M., 1988. *Proc. of a Workshop on Broad-band Downhole Seismometers in the Deep Ocean.* Woods Hole Oceanographic Institution.

Scientific Party, 1980. *Init. Repts. DSDP,* 56, 57: Washington (U. S. Govt. Printing Office).

Suyehiro, K., Kaiho, Y., Nishizawa, A., Kanazawa, T., and Shimamura, H., 1990. Seismic upper crust of the Japan Trench inner slope. *Tohoku Geophys. J.,* 33:281–305.

Suyehiro, K., Kanazawa, T., Nishizawa, A., and Shimamura, H., 1985a. Crustal structure beneath the inner trench slope of the Japan Trench. *Tectonophysics,* 112:155–191.

Suyehiro, K., Kanazawa, T., and Shimamura, H., 1985b. Air gun-ocean bottom seismograph seismic structure across the Japan Trench area. *In* Kagami, H., Karig, D.E., Coulbourn, W.T., et al., *Init. Repts. DSDP,* 87: Washington (U.S. Govt. Printing Office), 751–755.

Suyehiro, K., and Nishizawa, A., 1994. Crustal structure and seismicity beneath the forearc off northeastern Japan. *J. Geophys. Res.,* 99:22331–22348.

Tanioka, Y., and Satake, K., 1996. Fault parameters of the 1896 Sanriku tsunami earthquake estimated from tsunami numerical modeling. *Geophys. Res. Lett.,* 23:1549–1552.

von Huene, R., Klaeschen, D., Cropp, B., and Miller, J., 1994. Tectonic structure across the accretionary and erosional parts of the Japan Trench margin. *J. Geophys. Res.,* 99:22349–22361.

von Huene, R., and Lallemand, S., 1990. Tectonic erosion along the Japan and Peru convergent margins. *Geol. Soc. Am. Bull.,* 102:704–720.

von Huene, R., Langseth, M., Nasu, N., and Okada, H., 1982. A summary of Cenozoic tectonic history along IPOD Japan Trench transect. *Geol. Soc. Am. Bull.,* 93:829–846.

von Huene, R., Nasu, N., Arthur, M., Cadet, J.P., Carson, B., Moore, G.W., Honza, E., Fujioka, K., Barron, J.A., Keller, G., Reynolds, R., Shaffer, B.L., Sato, S., and Bell, G., 1978. Japan Trench transected on Leg 57. *Geotimes,* 23:16–21.

Figure F1. Location of Leg 186 sites. Contours shown at 1000-m intervals. Sites 1150 and 1151 are situated at the deep-sea terrace landward of the Japan Trench.

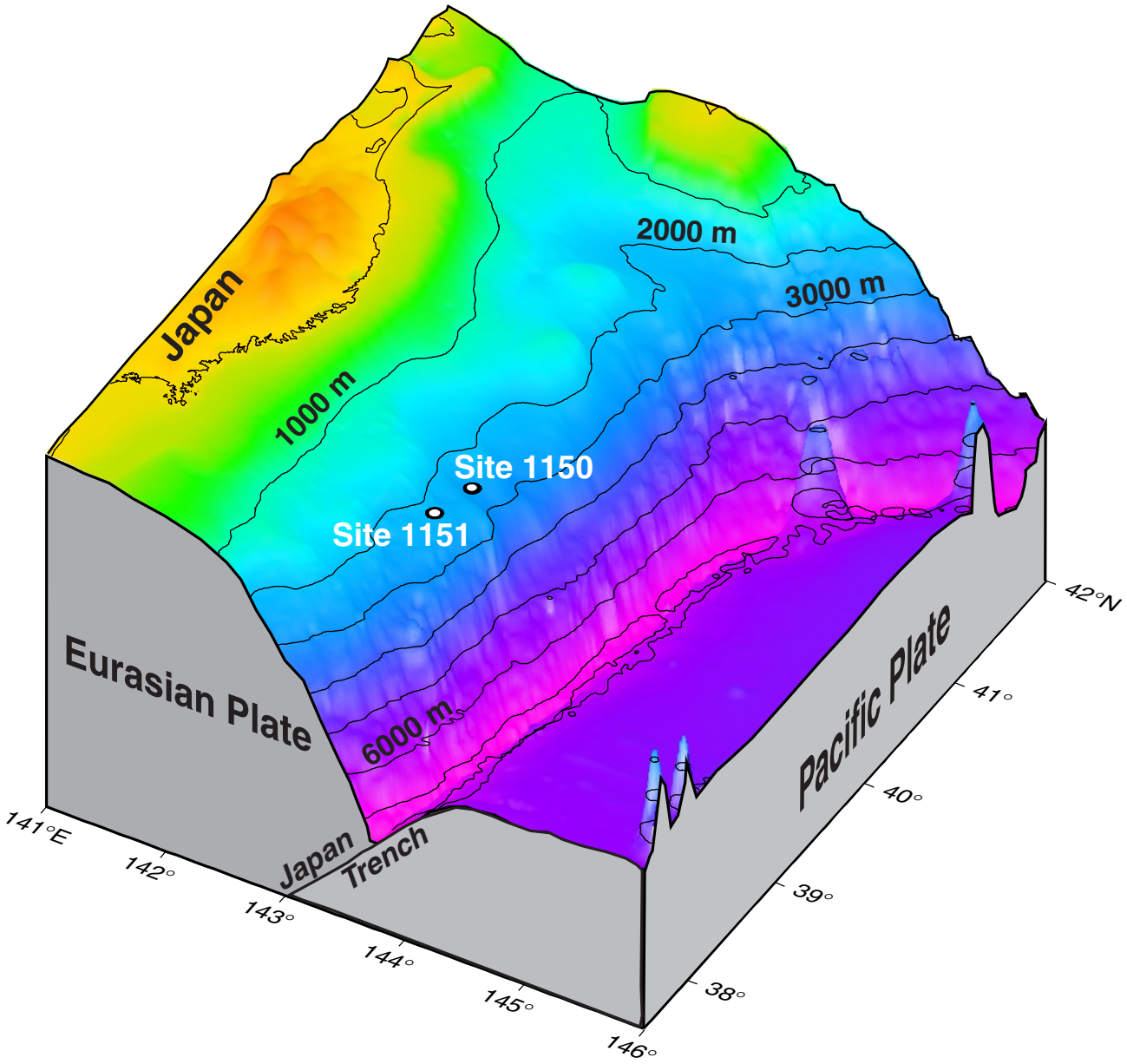

Figure F2. Map of the Japan Trench area off northeast Japan showing ODP Leg 186 Sites 1150 and 1151; previous drilling sites from DSDP Legs 56, 57, and 87; and seismic lines.

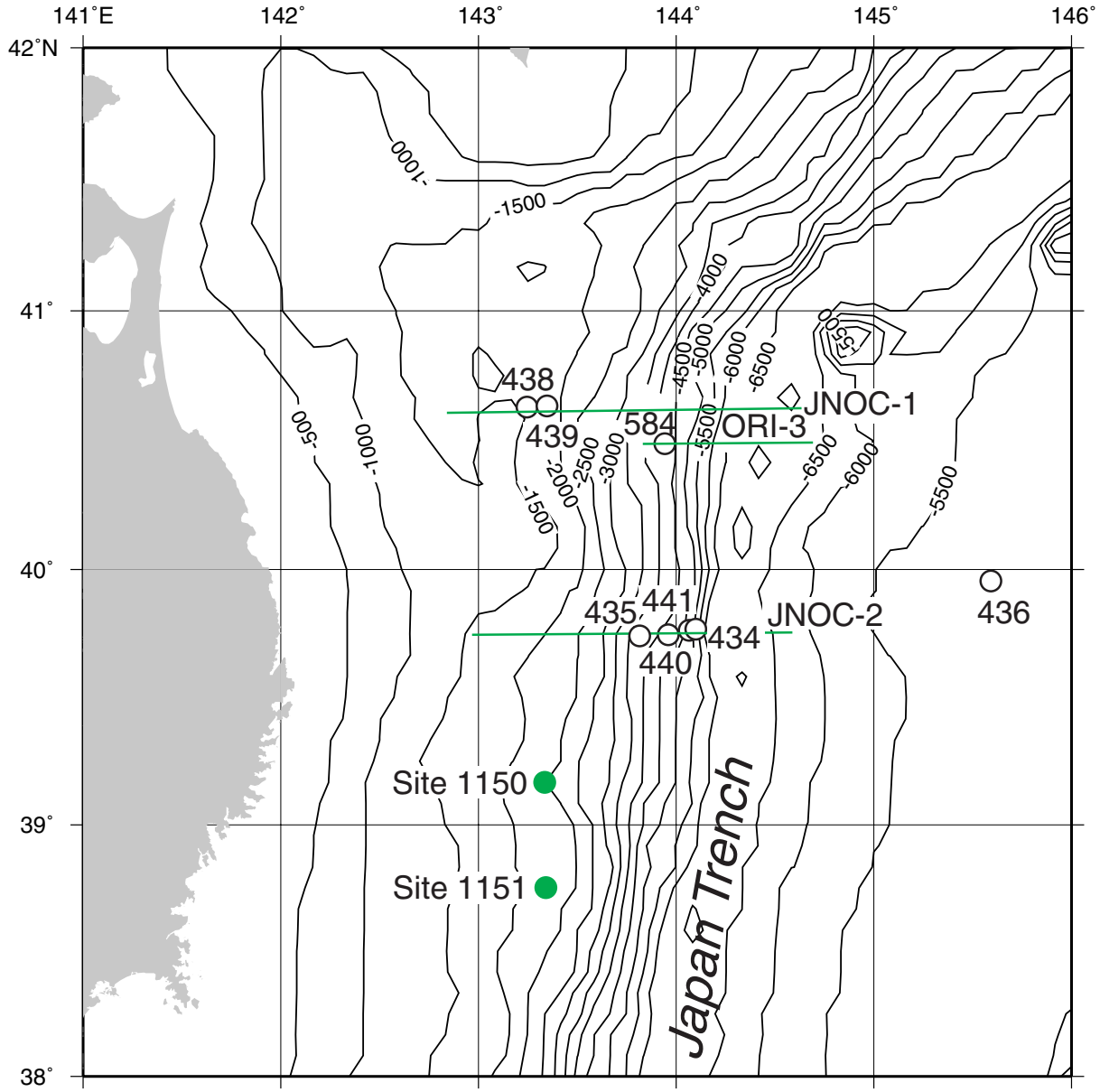

Figure F3. Schematic cross section of the Japan Trench-arc system (from Suyehiro and Nishizawa, 1994).

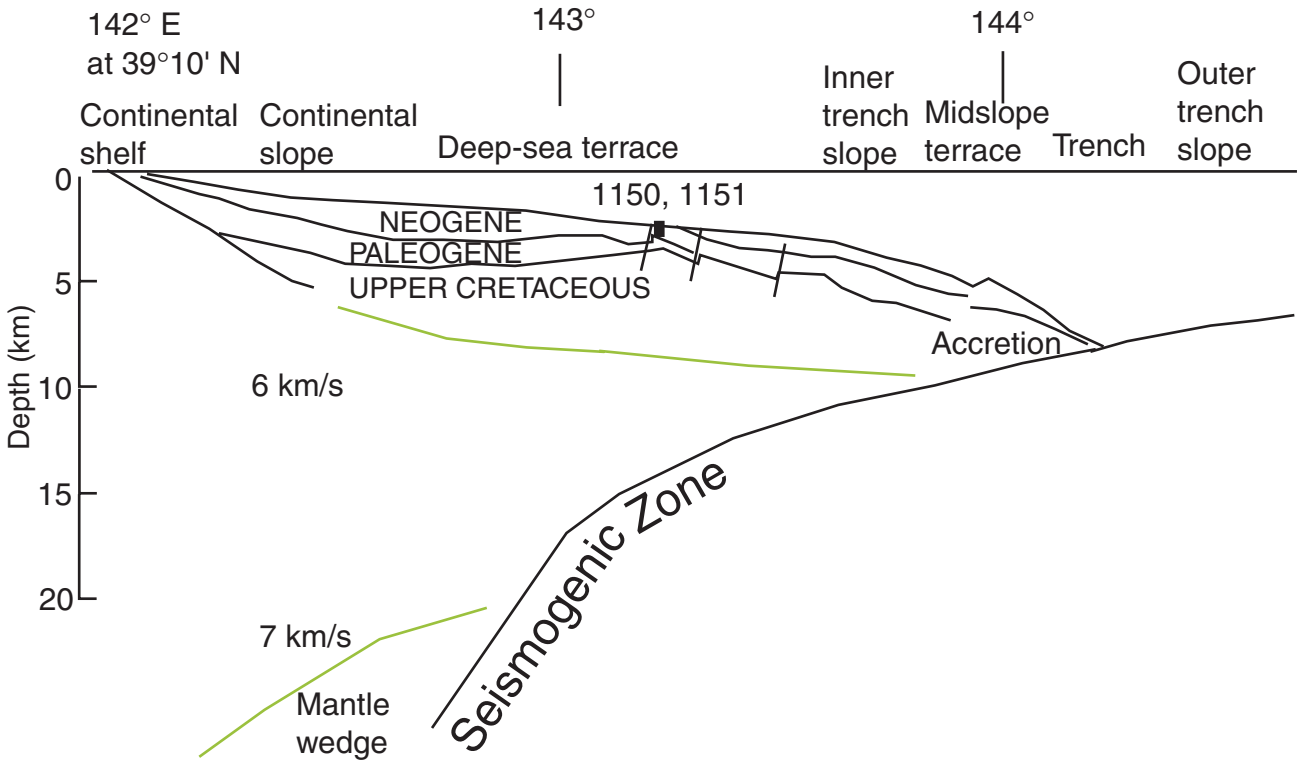

Figure F4. An example of a seismic record section across the Japan Trench showing characteristic features of this area.

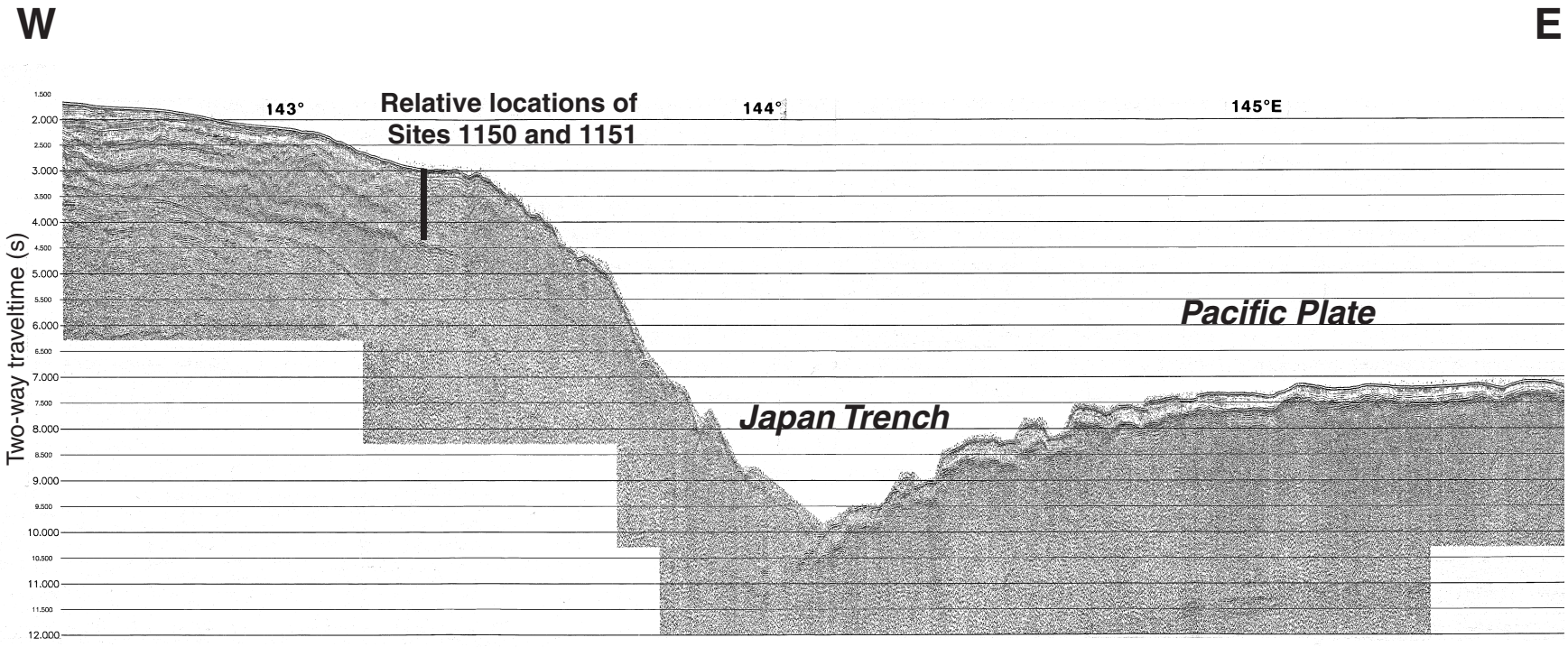

Figure F5. A model of tectonic subsidence history (from von Huene and Lallemand, 1990).

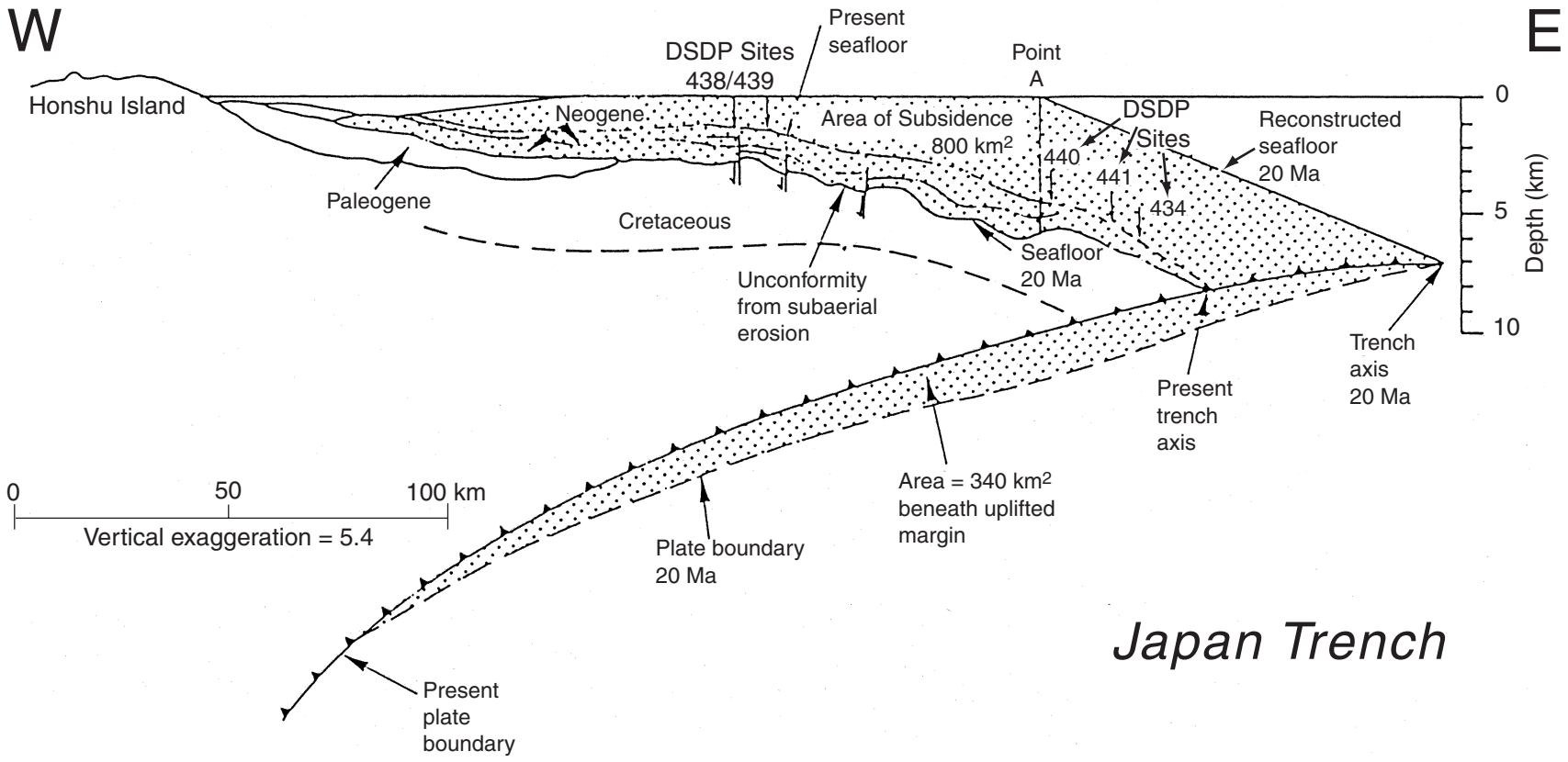

Figure F6. Epicenters of large thrust earthquakes. An M7 class earthquake can rupture an area on the order of 1000 km^2, dislocating ~1 m.

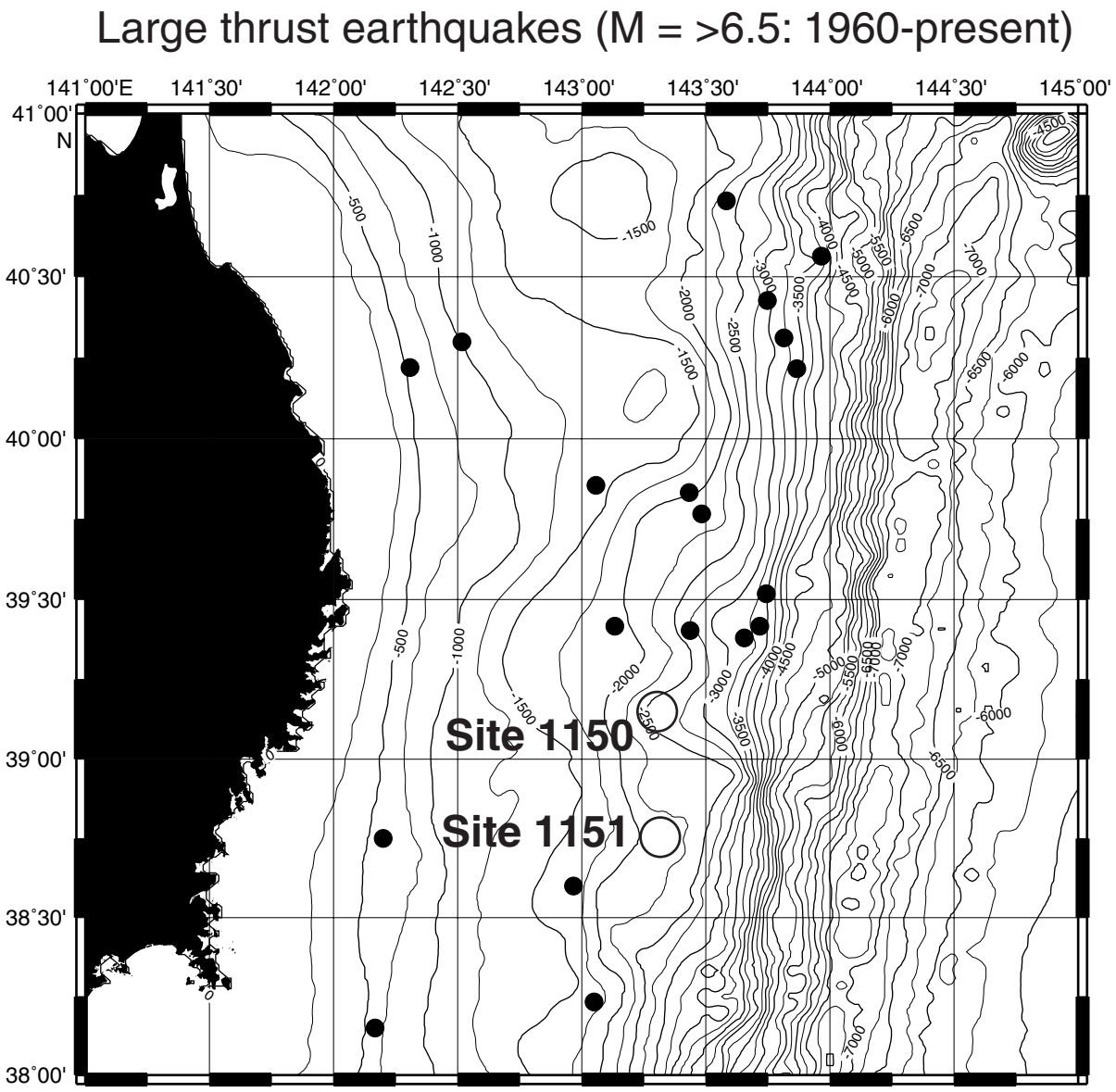

Figure F7. Map of Japan Trench area with seismicity (R. Hino, pers. comm., 1998). The locations of proposed Sites 1150 and 1151 are shown. Focal depth symbols: open circle = 0–10 km; open square = 10–20 km; open triangle = 20–30 km; solid circle = 30–40 km; solid square = 40–50 km; solid triangle = >50 km.

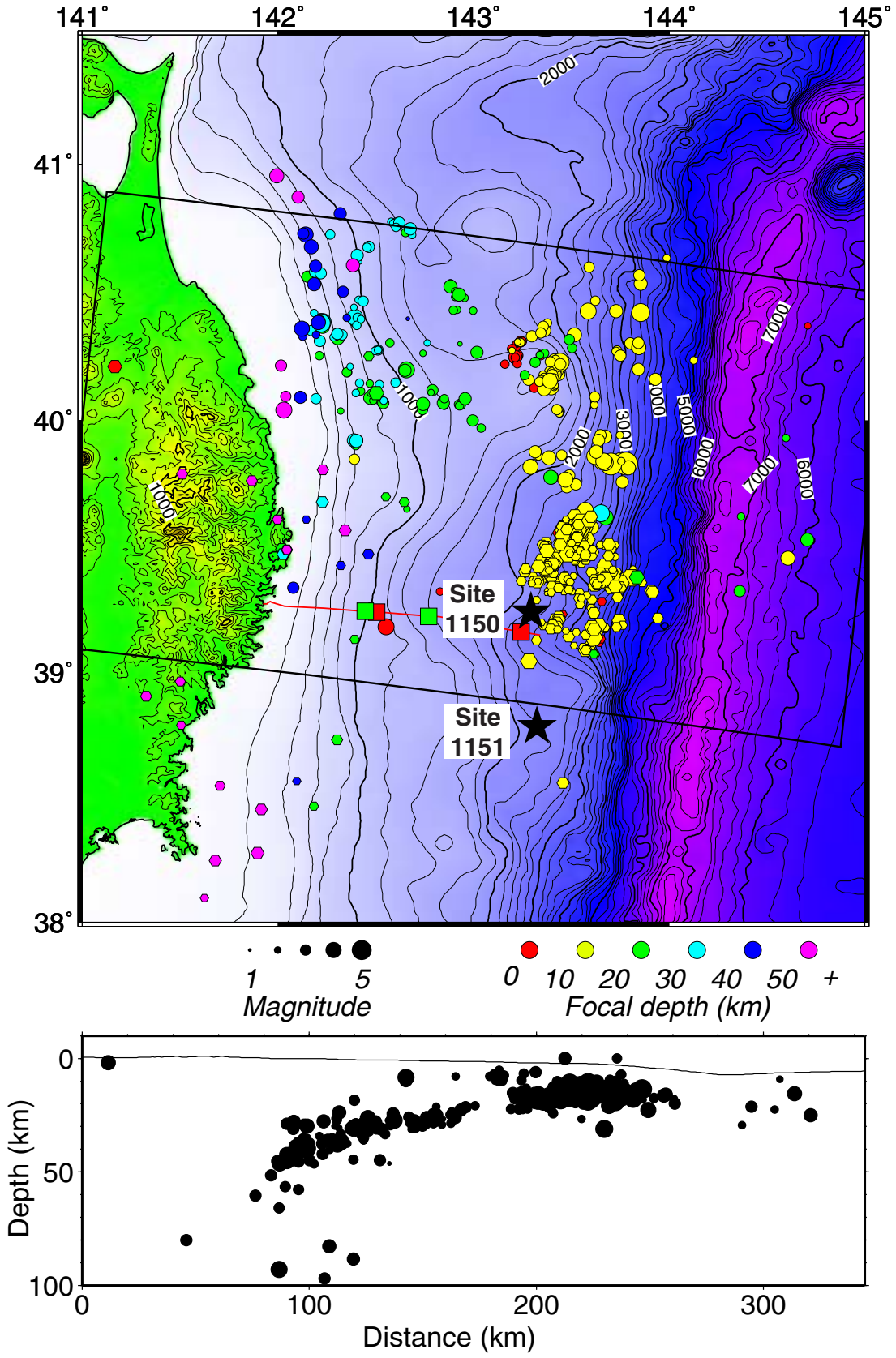

Figure F8. Schematic of the seafloor and borehole installation for Hole 1150D. The reentry cone is installed and the casing cemented in. The instrument string is coupled to 4½-in casing pipe and to the hanger/riser. This is inserted into the hole using the drill string. Cement is pumped through the instrument string and up into the cased part of the hole. The battery frame is then lowered onto the reentry cone, and the hanger/riser is then decoupled from the drill string. mbrf = meters below rig floor, TD = total depth.

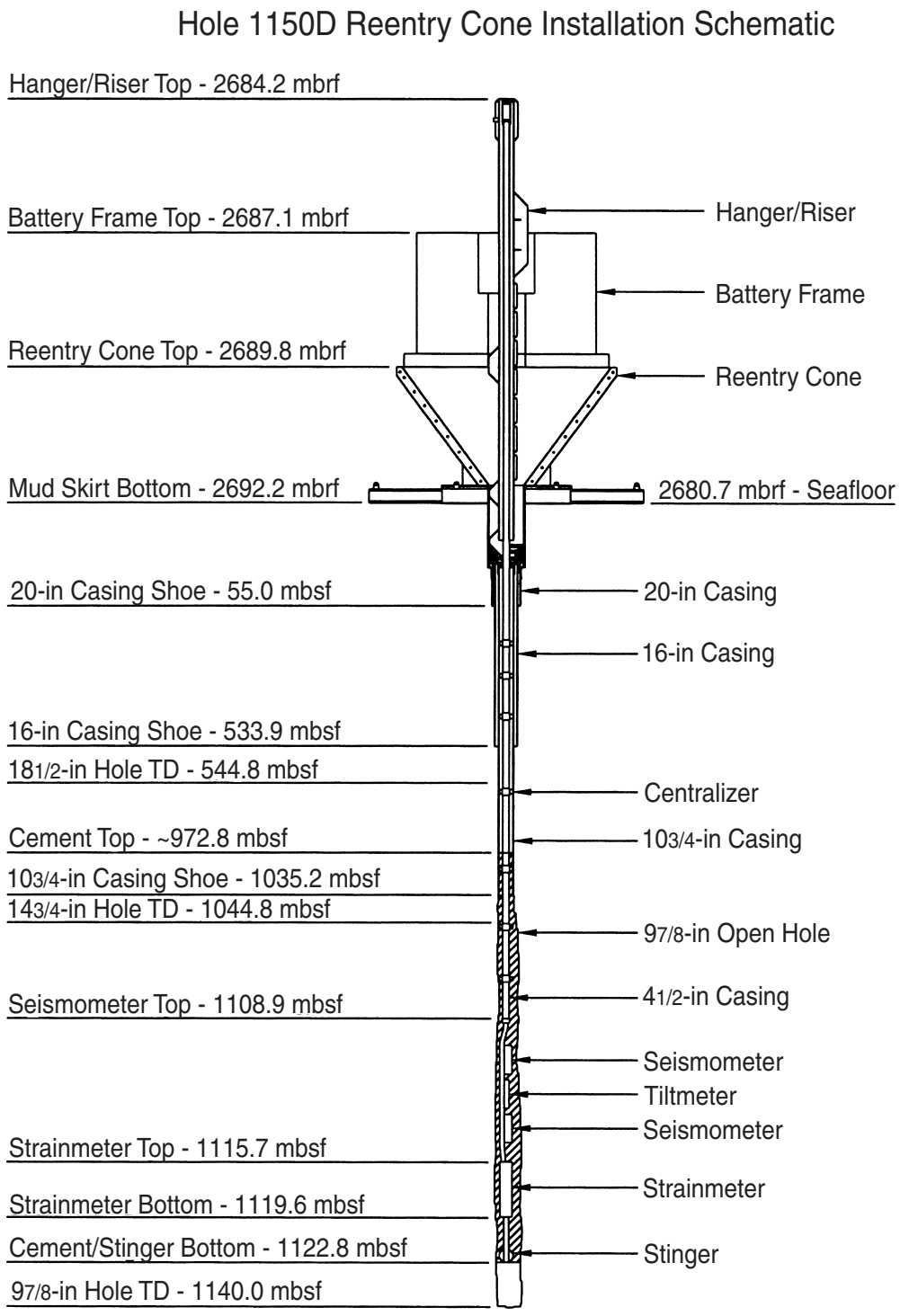

Figure F9. Schematic of the seafloor and borehole installation for Hole 1151B. Layout and abbreviations as for Hole 1150D in Figure F8, p. 26. The open hole is half the length of that in Hole 1150D.

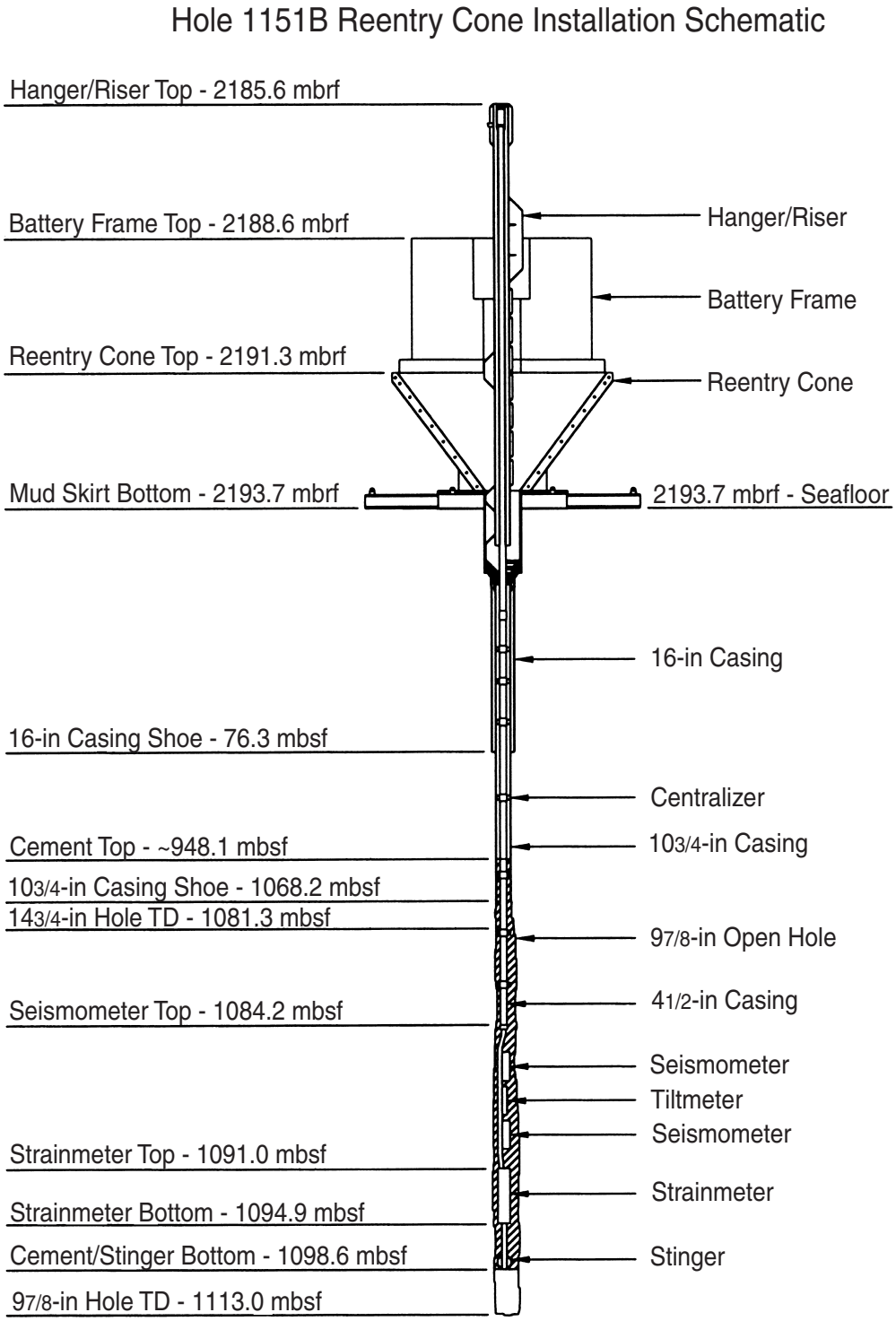

Figure F10. VIT camera images of the successfully deployed battery pack as it sits on top of the reentry cone at Hole 1150D. The image was taken while the drill pipe and the J-type running tool were still attached to the instrument string.

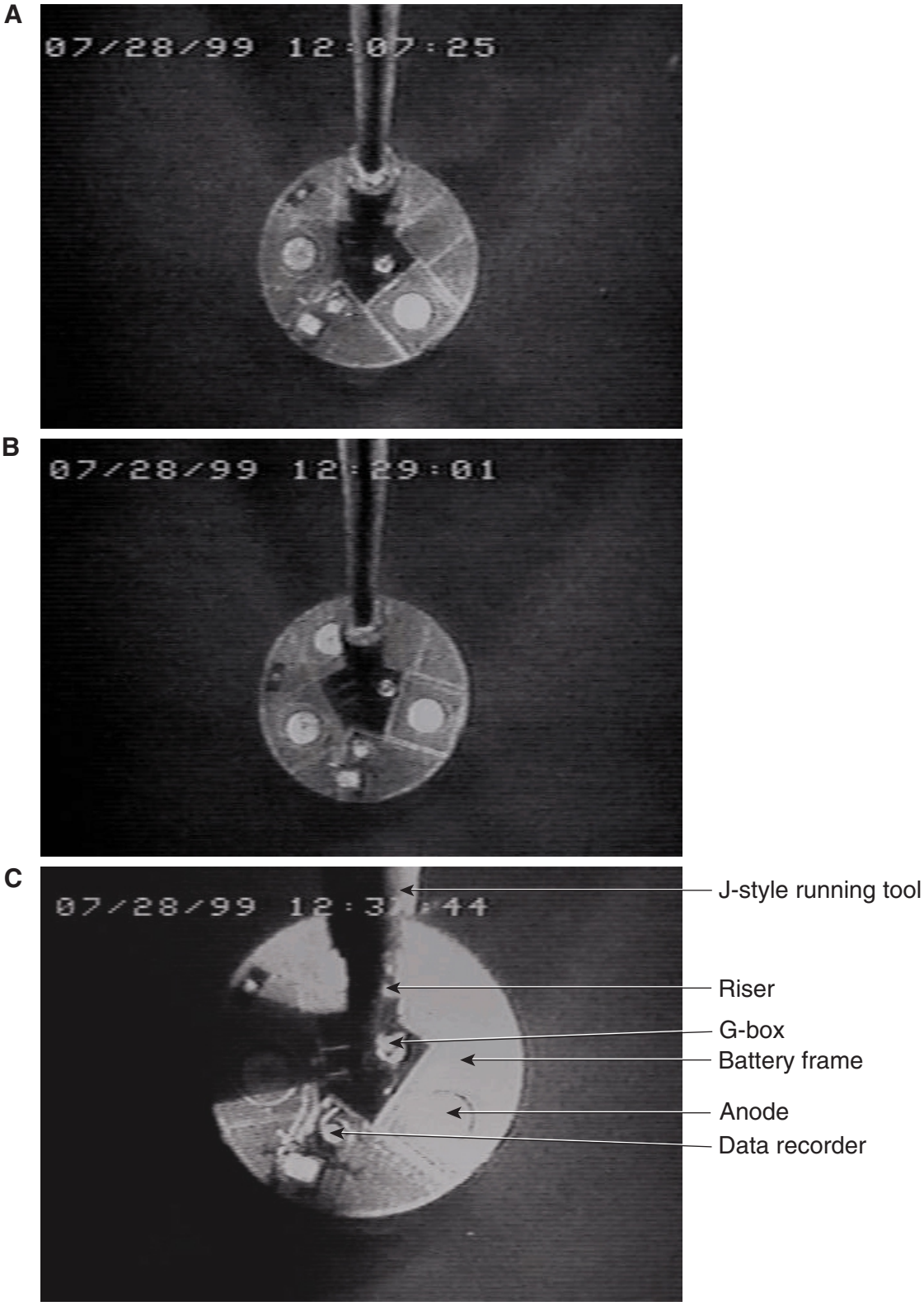

Figure F11. Lithostratigraphic summary for Sites 1150 and 1151. (Continued on next page.)

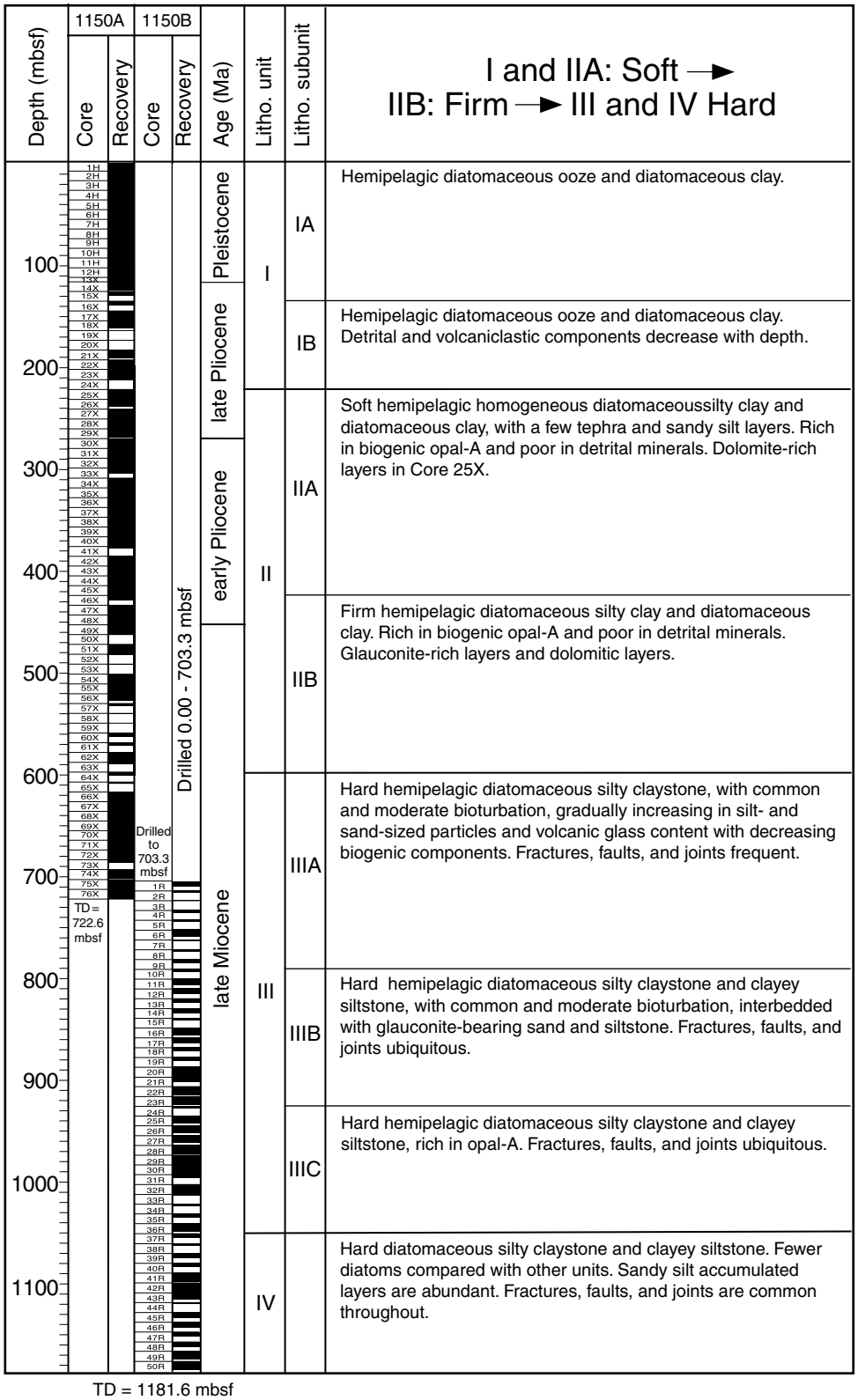

Figure F11 (continued).

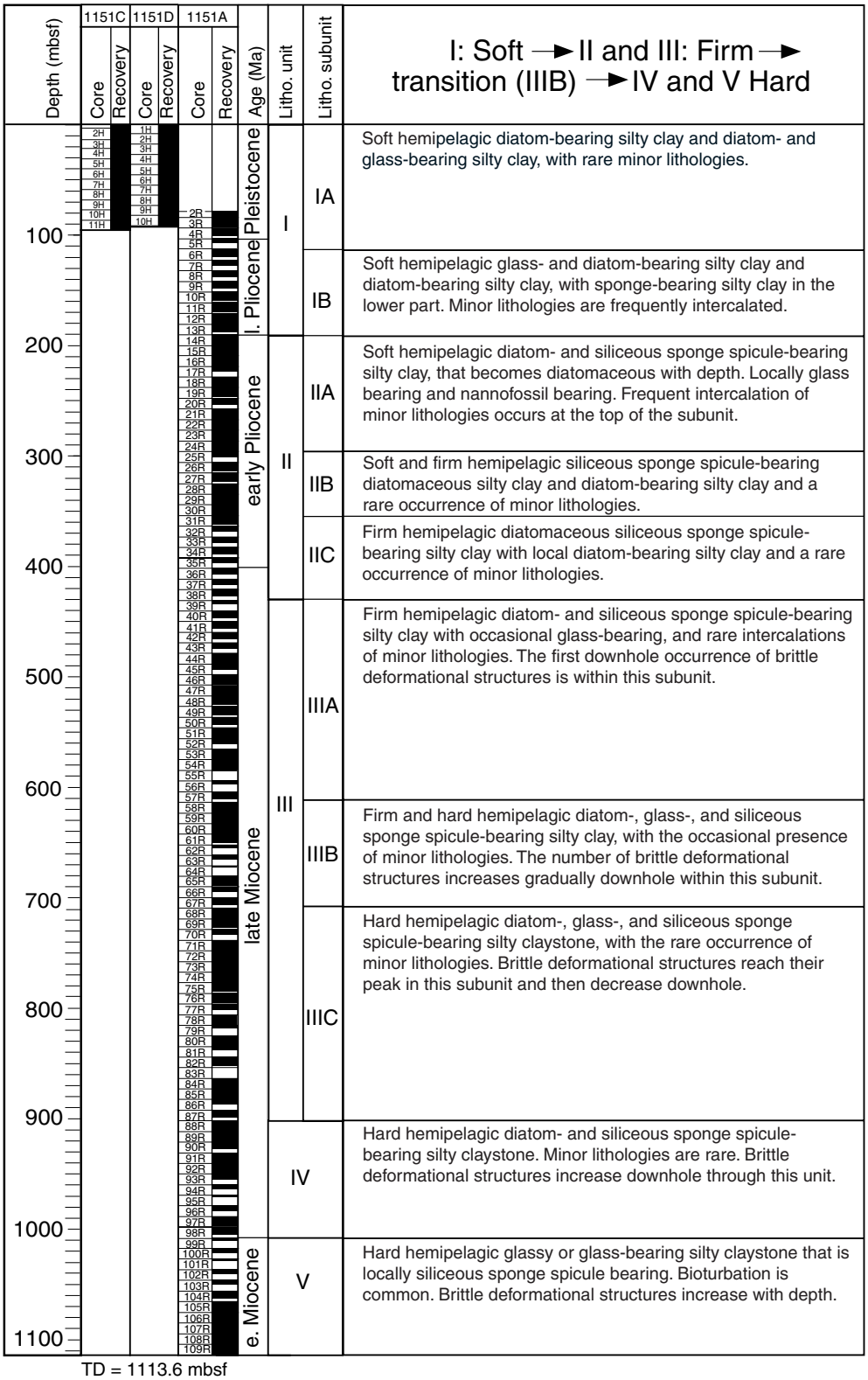

Figure F12. Chlorinity change in interstitial water. Data from this leg are compared with the ODP Leg 128 Sea of Japan (Site 799) and DSDP Leg 57 Japan Trench (Site 438) results.

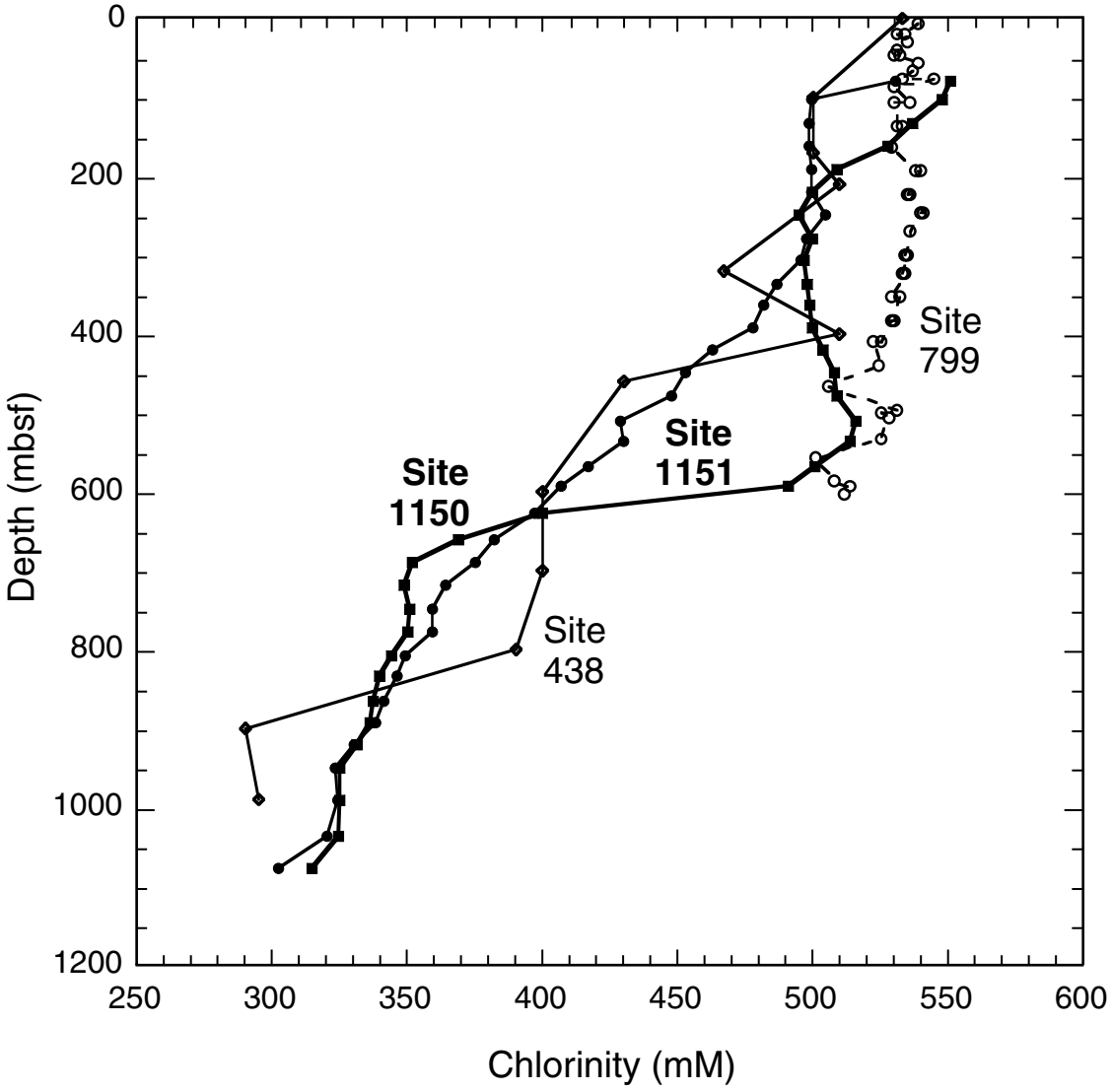

Figure F13. Age-depth curves for Leg 186 sites and other Japan Trench sites. The geomagnetic polarity time scale is also shown.

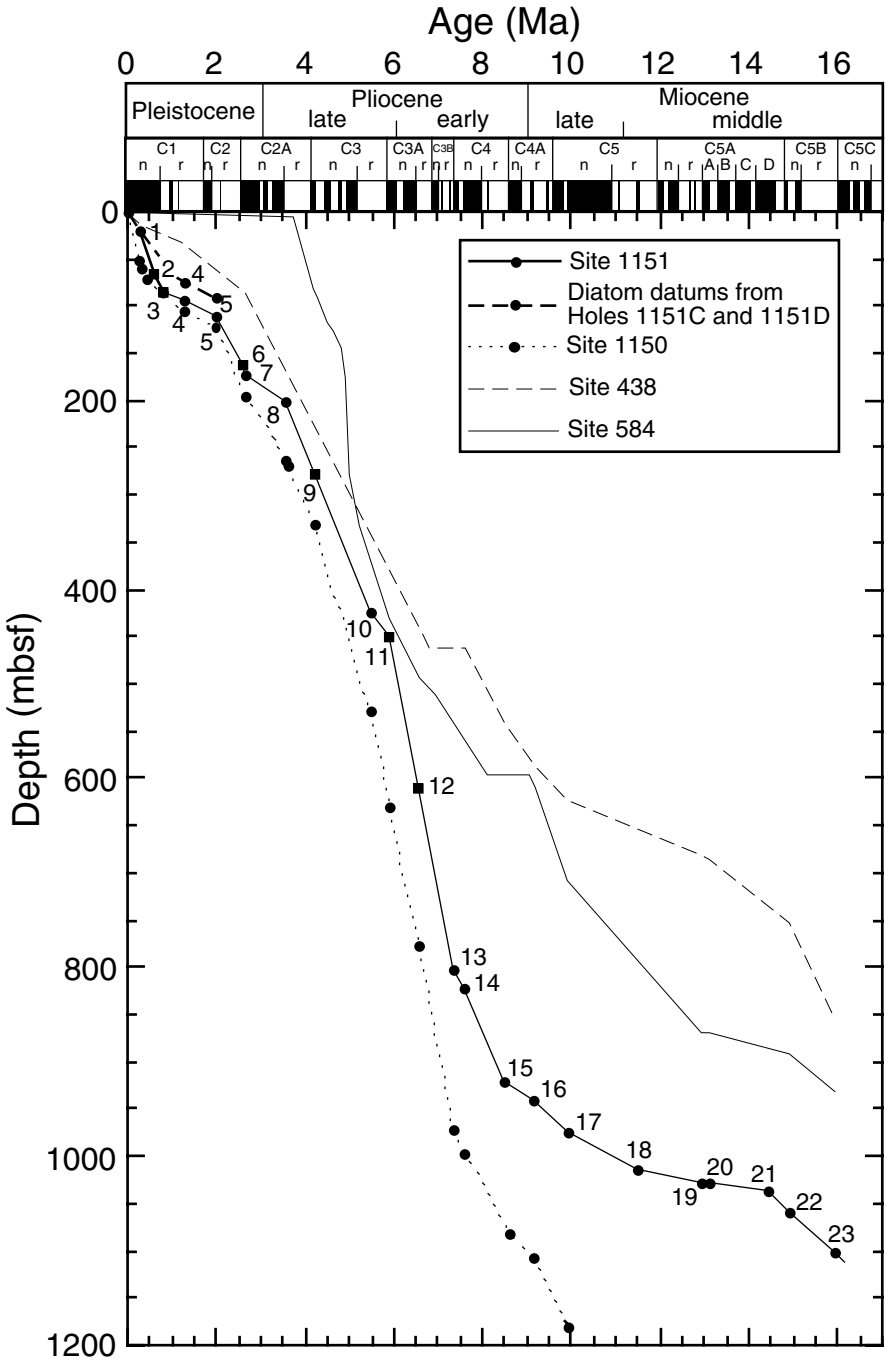

Figure F14. Smoothed curve presentation of sedimentation rates along the Japan Trench.

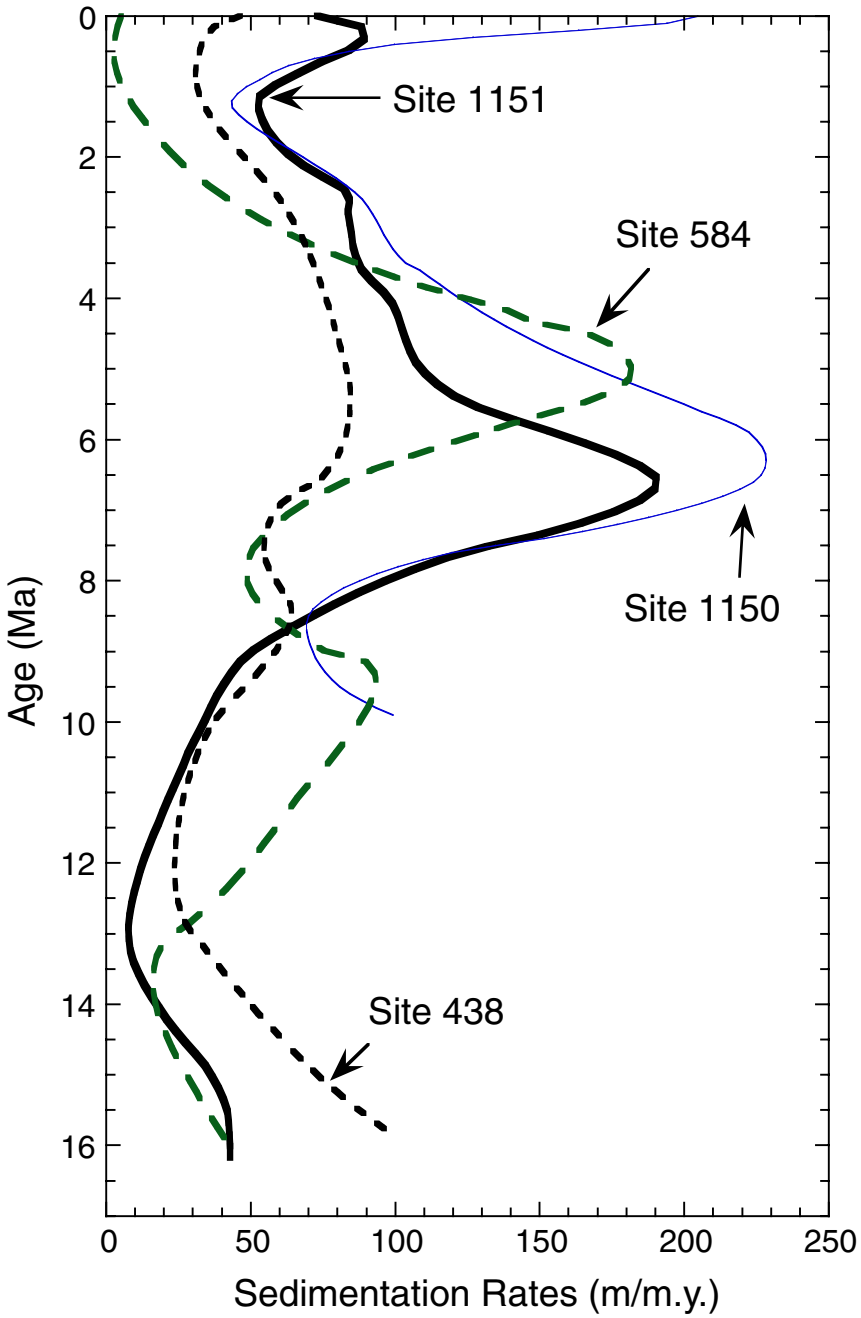

Figure F15. Ash records from Leg 186 compared with other Japan Trench sites.

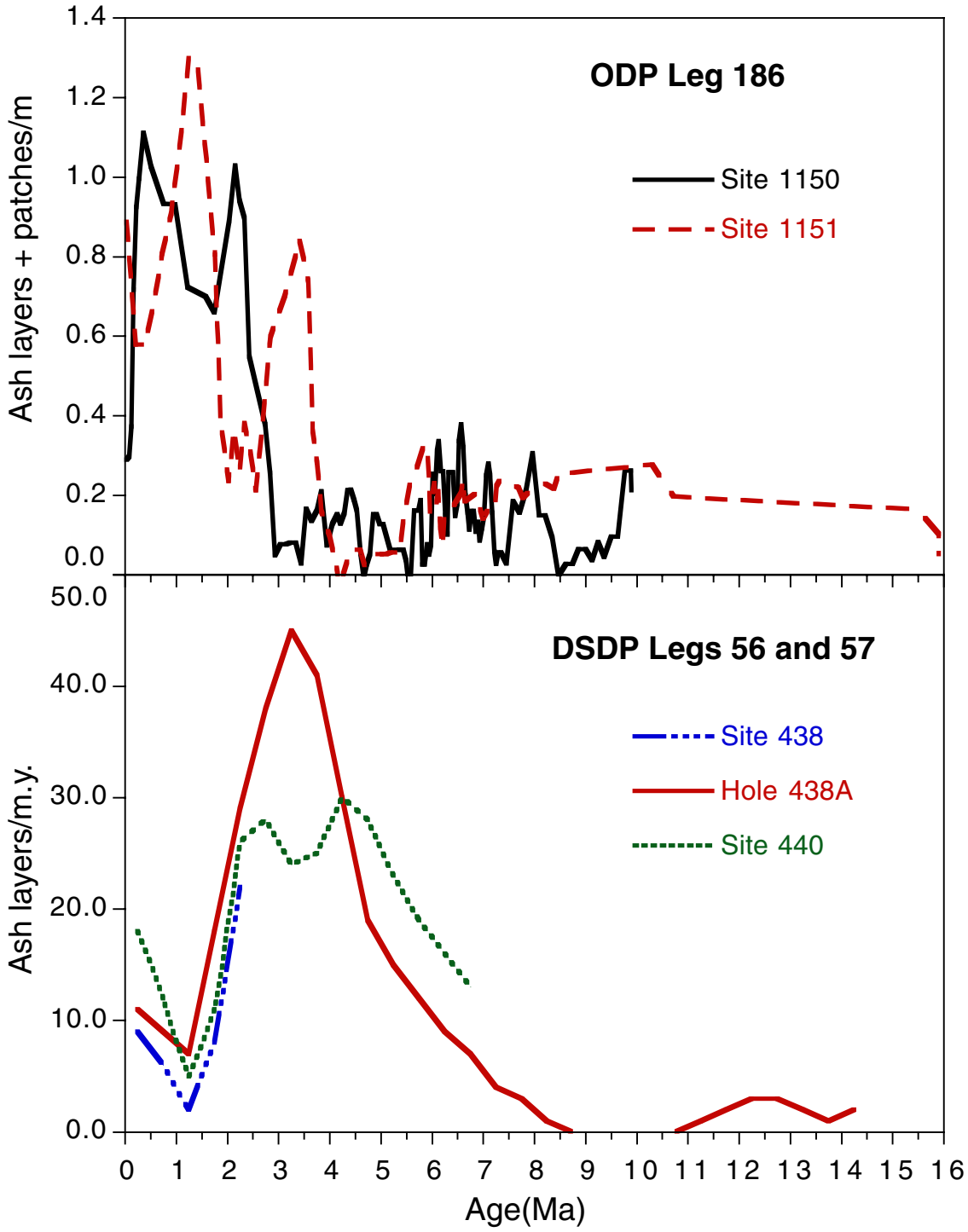

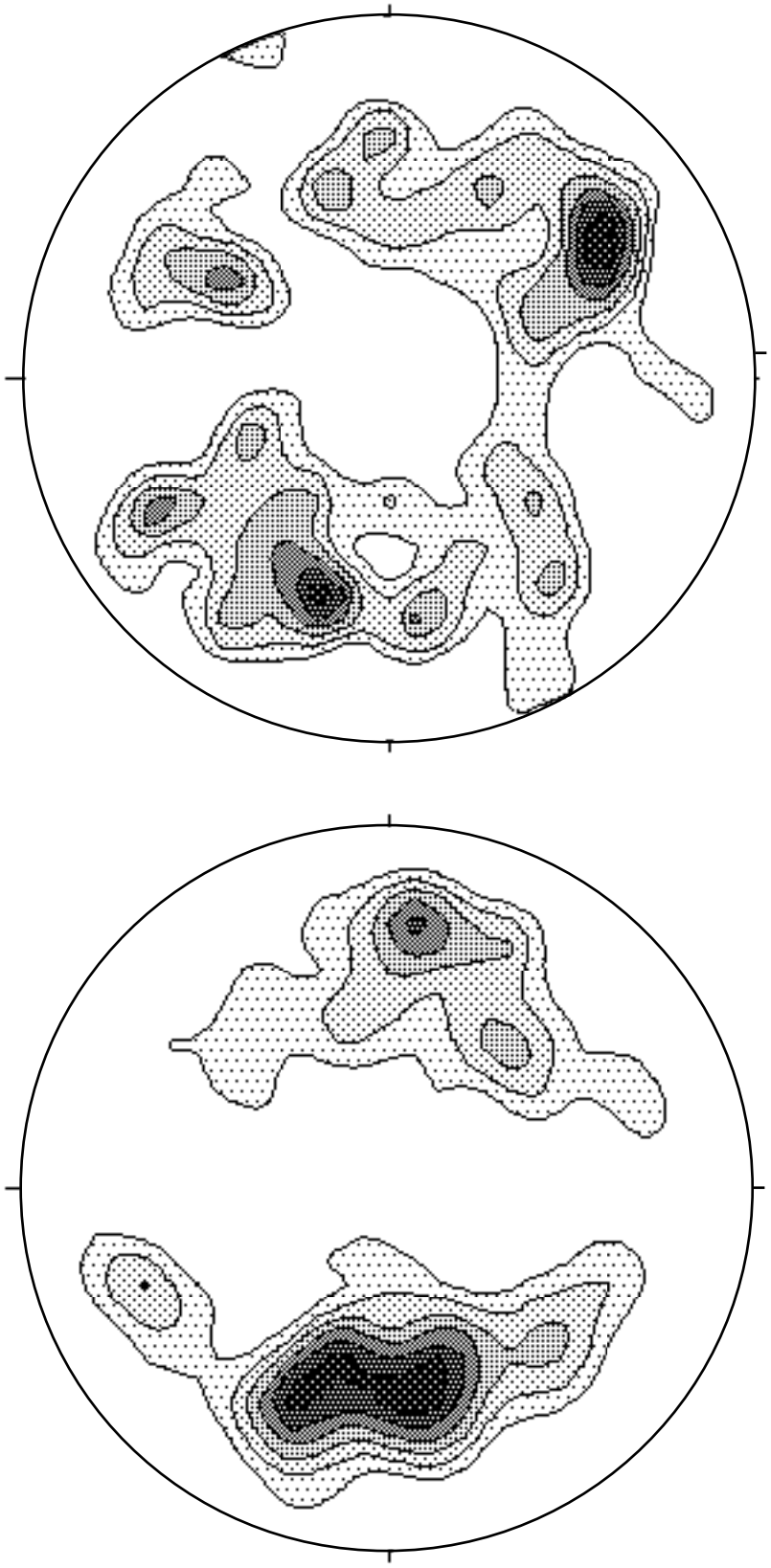

Figure F16. Fault orientations. **A.** Hole 1150B. **B.** Hole 1151A.

Figure F17. Frequency of faults at Sites 1150 and 1151.

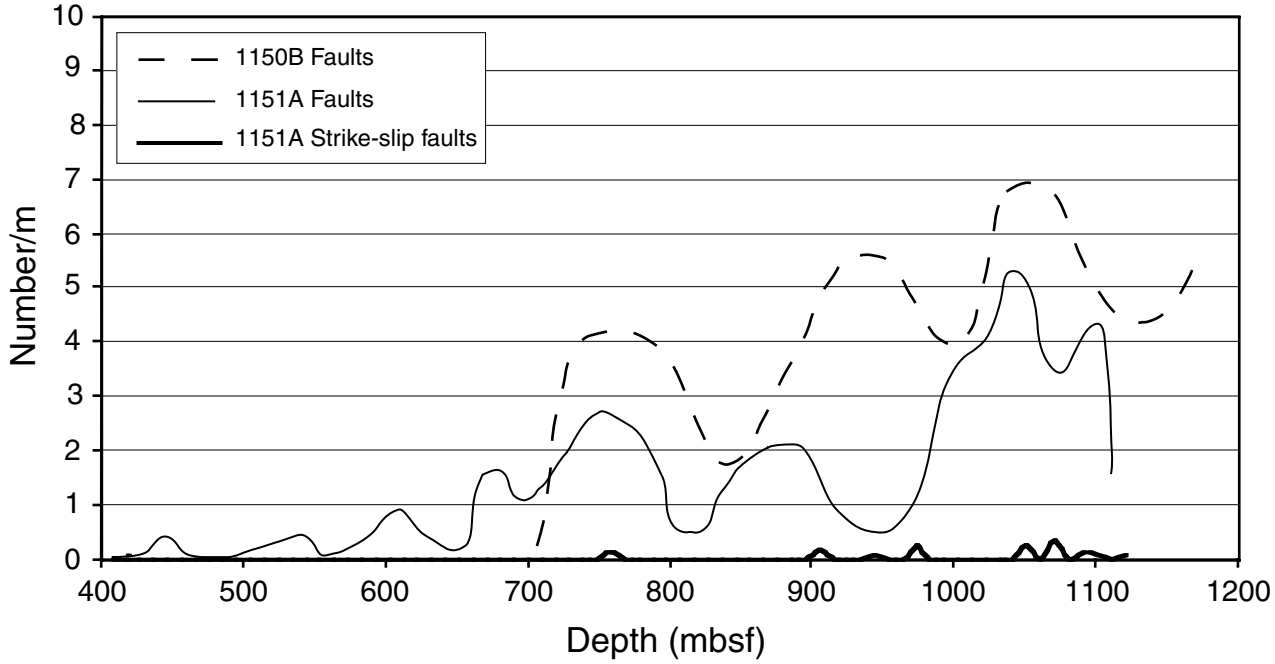

Table T1. Leg 186 operational summary.

Hole	Latitude	Longitude	Water depth (m)	Number of cores	Interval cored (m)	Core recovered (m)	Recovery (%)	Interval drilled (m)	Maximum penetration (m)
1150A	39°10.9148′N	143°19.9155′E	2680.8	76	722.6	566.40	78.38	0.0	722.6
1150B	39°10.9145′N	143°19.9470′E	2680.8	50	478.3	269.39	56.32	703.3	1181.6
1150C	39°10.9172′N	143°19.8942′E	2680.7	0	0.0	0.00	0.00	1050.0	1050.0
1150D	39°10.9172′N	143°19.8942′E	2680.7	0	0.0	0.00	0.00	1139.8	1139.8
Site 1150 totals:	39°10.9159′N	143°19.9127′E	2680.7	126	1200.9	835.79	69.60	2893.1	1181.6
1151A*	38°45.1195′N	143°20.0642′E	2182.2	108	1035.6	707.57	68.32	78.0	1113.6
1151B	38°45.1244′N	143°20.0147′E	2181.6	0	0.0	0.00	0.00	1113.0	1113.0
1151C	38°45.0202′N	143°20.0425′E	2174.2	11	97.2	101.75	104.68	0.0	97.2
1151D	38°45.0138′N	143°20.0441′E	2171.9	10	93.0	96.19	103.43	781.0	874.0
Site 1151 totals:	38°45.0695′N	143°20.0414′E	2177.5	129	1225.8	905.51	73.87	1972.0	1113.6
Leg 186 totals:				255	2426.7	1741.30	71.76	4865.1	1181.6

Table T1 (continued).

Hole	Arrival date and time (local)	Departure date and time (local)	Time on hole (hr)	Number of APC cores	Number of XCB cores	Number of RCB cores	Seafloor depth (mbrf)	Total drill string length (mbrf)
1150A	22 June 1999 18:30	26 June 1999	99.75	12	64	0	2692.2	3414.8
1150B	26 June 1999 22:15	3 July 1999	159.25	0	0	50	2692.2	3873.8
1150C	23 July 1999 15:30	23 July 1999	7.00	0	0	0	2692.2	3742.2
1150D	23 July 1999 22:30	28 July 1999	116.50	0	0	0	2692.2	3832.0
Site 1150 totals:			382.50	12	64	50	2692.2	3715.7
1151A*	28 July 1999 22:00	2 Aug 1999	115.75	0	0	108	2193.7	3307.3
1151B	2 Aug 1999 17:45	9 Aug 1999	168.00	0	0	0	2193.7	3306.7
1151C	9 Aug 1999 17:45	10 Aug 1999	16.00	11	0	0	2186.3	2283.5
1151D	10 Aug 1999 9:45	12 Aug 1999	61.75	10	0	0	2184.0	3058.0
Site 1151 totals:			361.50	21	0	108	2189.4	2988.9
Leg 186 totals:			744.00	33	64	158	2440.8	3352.3

Note: * = totals do not include a wash core (186-1151A-1W) collected at the top of Hole 1151A.